

¹ **GLO-Roots: an imaging platform enabling multidimensional characterization of soil-grown roots systems**

³ Rubén Rellán-Álvarez^{1, 9}, Guillaume Lobet², Heike Lindner^{1, 8}, Pierre-Luc Pradier^{1, 8, 10},
⁴ Jose Sebastian^{1, 8}, Muh-Ching Yee¹, Yu Geng^{1, 7}, Charlotte Trontin¹, Therese LaRue³,
⁵ Amanda Schrager-Lavelle⁴, Cara H. Haney⁵, Rita Nieu⁶, Julin Maloof⁴, John P. Vogel⁷,
⁶ José R. Dinneny^{1, 12}

⁷ ¹ Department of Plant Biology, Carnegie Institution for Science, Stanford, CA, USA.

⁸ ² PhytoSystems, University of Liège, Liège, Belgium.

⁹ ³ Department of Biology, Stanford University, Stanford, CA, USA.

¹⁰ ⁴ Department of Plant Biology, UC Davis, Davis, CA, USA.

¹¹ ⁵ Harvard Medical School, Massachusetts General Hospital, Department of Genetics, De-
¹² partment of Molecular Biology Boston, MA, USA

¹³ ⁶ USDA Western Regional Research Center, Albany, CA, USA

¹⁴ ⁷ DOE Joint Genome Institute, Walnut Creek, CA, USA

¹⁵ ⁸ These authors contributed equally

¹⁶ ⁹ Present address: Laboratorio Nacional de Genómica para la Biodiversidad (Langebio),
¹⁷ Unidad de Genómica Avanzada, Centro de Investigación y de Estudios Avanzados del Insti-
¹⁸ tuto Politécnico Nacional (CINVESTAV-IPN), Irapuato, Guanajuato, México

¹⁹ ¹⁰ Present address: Boyce Thompson Institute for Plant Research/USDA, Ithaca, NY, USA.

²⁰ ¹¹ Present address: Energy Biosciences Institute, UC, Berkeley, CA, USA

²¹ ¹² Corresponding author

²² **Author contributions:**

²³ RR-A: Conception, design and development of the growth and imaging system and Arabidop-
²⁴ sis transgenic lines; acquisition, analysis and interpretation of data; drafting and revising

25 the article.

26 GL: Development of the GLO-RIA image analysis plugin, analysis and interpretation of

27 data, drafting and revising the article.

28 HL: Acquisition of data, development of the tomato growth and imaging setup.

29 P-LP: Acquisition of data, analysis and interpretation of data

30 JS: Development of Brachypodium transgenic lines, acquisition and analysis of Brachy-

31 podium, Arabidopsis and tomato data.

32 MCY: Development of Arabidopsis and Brachypodium transgenic lines.

33 YG: Development of Arabidopsis transgenic lines.

34 CT: Acquisition and analysis of the QPCR data

35 TL: Acquisition and analysis of the QPCR data

36 AS-L: Contributed the unpublished dual-color tomato line.

37 CH: Contributed the unpublished *Pseudomonas fluorescens* CH267-lux strain.

38 RN: Contribution to the development of the Brachypodium transgenic line.

39 JM: Contributed the unpublished dual-color tomato line.

40 JPV: Contribution to the development of the Brachypodium transgenic line.

41 JRD: Conception, design and development of the growth and imaging system and Arabidop-

42 sis transgenic lines; acquisition, analysis and interpretation of data; drafting and revising

43 the article.

44 All authors read and approve the final version of the manuscript.

45 **Abstract**

46 Root systems develop different root types that individually sense cues from their local

47 environment and integrate this information with systemic signals. This complex multi-

48 dimensional amalgam of inputs enables continuous adjustment of root growth rates, direc-
49 tion and metabolic activity that define a dynamic physical network. Current methods for
50 analyzing root biology balance physiological relevance with imaging capability. To bridge
51 this divide, we developed an integrated imaging system called Growth and Luminescence
52 Observatory for Roots (GLO-Roots) that uses luminescence-based reporters to enable stud-
53 ies of root architecture and gene expression patterns in soil-grown, light-shielded roots. We
54 have developed image analysis algorithms that allow the spatial integration of soil prop-
55 erties such as soil moisture with root traits. We propose GLO-Roots as a system that
56 has great utility in presenting environmental stimuli to roots in ways that evoke natural
57 adaptive responses and in providing tools for studying the multi-dimensional nature of such
58 processes.

59 **Introduction**

60 Plant roots are three-dimensional assemblies of cells that coordinately monitor and acclimate
61 to soil environmental change by altering physiological and developmental processes through
62 cell-type and organ-specific regulatory mechanisms^{1,2}. Soil comprises a complex distribution
63 of particles of different size, composition and physical properties, airspaces, variation in
64 nutrient availability and microbial diversity^{3,4}. These physical, chemical and biological
65 properties of soil can vary on spatial scales of meters to microns, and on temporal scales
66 ranging from seasonal change to seconds. Root tips monitor this environment through
67 locally and systemically acting sensory mechanisms^{5,6}.

68 The architecture of the root system determines the volume of soil where resources can be
69 accessed by the plant (rhizosphere) and is under both environmental and genetic control.
70 Plasticity in growth parameters allows the plant to adjust its form to suit a particular soil.
71 Lateral roots, which usually make up the majority of the total root system, often grow at an
72 angle divergent from the gravity vector. This gravity set-point angle (GSA) is controlled by
73 auxin biosynthesis and signaling and can be regulated by developmental age and root type⁷.
74 Recent cloning of the *DRO1* Quantitative Trait Locus (QTL) demonstrates that natural

75 genetic variation is a powerful tool for uncovering such control mechanisms⁸.

76 Specific root ideotypes (idealized phenotypes) have been proposed to be optimal for acquisition
77 of water and nitrogen, which are distinct from ideotypes for low phosphorus. Based on
78 computational modeling and field studies, the “steep, deep and cheap” ideotype proposed by
79 Lynch and colleagues may provide advantages to the plant for capturing water and elements
80 like nitrogen that are water soluble and therefore tend to move in the soil column with water.
81 This ideotype consists of highly gravitropic, vertically oriented roots that grow deep in the
82 soil column and develop large amounts of aerenchyma, which reduces the overall metabolic
83 cost of the root system³. Other nutrients, like phosphorus, which have limited water solubility and are tightly bound to organic matter, usually accumulate in the top layers of soil
84 and favor root systems that are more highly branched and shallow. The low-phosphorus
85 ideotype effectively increases root exploration at the top layers of soil³. Modeling of root
86 system variables shows that optimum architecture for nitrogen and phosphorus uptake are
87 not the same⁹ and suggests tradeoffs that may affect the evolution of root architecture as a
88 population adapts to a particular environmental niche.

89

90 Clearly, understanding the architecture of root systems and how environmental conditions
91 alter root developmental programs is important for understanding adaptive mechanisms of
92 plants and for identifying the molecular-genetic basis for different response programs. In
93 addition, root systems have complexity beyond their architecture that needs to be incorporated
94 into our understanding of plant-environment interactions. Primary and lateral roots
95 exhibit different stress response programs in *Arabidopsis*² and may play specialized roles
96 in water and nutrient uptake. Thus, it is important to develop methods that allow for a
97 multidimensional characterization of the root system that includes growth, signaling, and
98 interactions with other organisms. Furthermore, physiological parameters that affect whole
99 plant responses to the environment, such as transpiration, are likely integrated into such
100 processes, thus requiring a more holistic approach to studies of root function.

101 Based on these considerations we have developed a new root imaging platform, Growth
102 and Luminescence Observatory for Roots (GLO-Roots), which allows root architecture and

103 gene expression to be studied in soil-grown plants. GLO-Roots is an integrated system
104 composed of custom growth vessels, luminescent reporters and imaging systems. We use
105 rhizotrons that have soil volumes equivalent to small pots and support growth of Arabidopsis
106 from germination to senescence. To visualize roots, we designed plant-codon optimized
107 luciferase reporters that emit light of different wavelengths. To visualize reporter expression,
108 plants are watered with a dilute luciferin solution and imaged afterwards. We have built
109 a custom luminescence imaging system that automatically captures images of rhizotrons
110 held vertically. The signal from each reporter is distinguished using band-pass filters held
111 in a motorized filter wheel, which enables automated acquisition of images from plants
112 expressing both structural and environmentally and developmentally responsive reporters.
113 We have also developed GLO-RIA (GLO-Roots Image Analysis), an ImageJ¹⁰ plugin that
114 allows for automated determination of root system area, convex hull, depth, width and
115 directionality, which quantifies the angle of root segments with respect to gravity. GLO-
116 RIA is also able to relate root system parameters to local root-associated variables such as
117 reporter expression intensity and soil-moisture content.

118 Overall GLO-Roots has great utility in presenting environmental stimuli to roots in phys-
119 iologically relevant ways and provides tools for characterizing responses to such stimuli at
120 the molecular level in whole adult root systems over broad time scales.

121 **Box 1.**

122 All resources for GLO-Roots, including the original raw data used in the manuscript, sample
123 images, GLO-RIA user manual, the latest software updates and the source code, can be
124 found at: <https://dinnenylab.wordpress.com/glo-roots/>

125 **Results**

126 We have developed an integrated platform for growing, imaging and analyzing root growth
127 that provides advances in physiological relevance and retains the ability to visualize aspects

¹²⁸ of root biology beyond structure.

¹²⁹ **The GLO-Roots platform**

¹³⁰ GLO-Roots is comprised of four parts: i) growth vessels called rhizotrons that allow plant
¹³¹ growth in soil and root imaging; ii) luminescent reporters that allow various aspects of root
¹³² biology to be tracked in living plants; iii) GLO1 luminescence-imaging system designed to
¹³³ automatically image rhizotrons; iv) GLO-RIA, an image analysis suite designed to quantify
¹³⁴ root systems imaged using GLO-Roots.

¹³⁵ **Plant growth system** GLO-Roots utilizes custom designed growth vessels classically
¹³⁶ known as rhizotrons, which hold a thin volume of soil between two sheets of polycarbon-
¹³⁷ ate plastic. Acrylic spacers provide a 2-mm space in which standard peat-based potting
¹³⁸ mix is added. Black vinyl sheets protect roots from light and rubber U-channels clamp
¹³⁹ the rhizotron materials together. Plastic racks hold the rhizotrons vertically and further
¹⁴⁰ protect the roots from light. Rhizotrons and rack are placed in a black tub and water are
¹⁴¹ added, to a depth of about 2 cm, at the bottom to maintain moisture in the rhizotrons
¹⁴² during plant growth. The volume of soil in the rhizotrons (100 cm^3) is similar to small pots
¹⁴³ commonly used for *Arabidopsis* and supports growth throughout the entire life cycle (Fig
¹⁴⁴ 1A-C and Supplement 1). To determine how the biology of plants grown in rhizotrons com-
¹⁴⁵ pares to other standard growth systems, we utilized high-throughput qRT-PCR to study
¹⁴⁶ how these conditions affect expression of 77 marker genes in root and shoot samples. These
¹⁴⁷ genes were curated from the literature and belong to a wide array of biological pathways
¹⁴⁸ including nutrient acquisition, hormone and light response and abiotic stress. Whole roots
¹⁴⁹ and shoot samples were collected at the end of the light and dark periods (Long-day condi-
¹⁵⁰ tions: 16 hour light, 8 hours dark) from plants grown in rhizotrons, pots, and petri dishes
¹⁵¹ with two different media compositions (1X Murashige and Skoog basal salts (MS), 1% su-
¹⁵² crose or 0.25X MS, no sucrose). Principal component analysis of the gene expression values
¹⁵³ showed a separation of soil and gel-grown root systems in the the first principal compo-
¹⁵⁴ nents (Figure 1-figure supplement 1A). In roots grown on gel-based media, we observed

enhanced expression of genes associated with light-regulated pathways (flavonoid biosynthesis: *FLAVINOL SYNTHASE1*, *FLS1*, *CHALCONE SYNTHASE*, *CHS* and photosynthesis: *RUBISCO SUBUNITS1A*, *RBCS1A*, *CYCLOPHILIN 38*, *CYP38*), which is expected due to the exposure of gel-grown roots to light. In addition, genes associated with phosphorus nutrition (*LOW PHOSPHATE RESPONSE1*, *LPR1*, *PHOSPHATE STARVATION RESPONSE1*, *PHR1*) were (Figure 1-figure table supplement 1) less expressed in soil-grown roots, suggesting differences in nutrient availability between the different growth systems. Interestingly, shoot samples were not clearly distinguished by growth media and, instead, time of day had a greater effect (Figure 1-Supplement 2). These data suggest root systems may be particularly sensitive to media conditions and indicate that rhizotron-grown root systems more closely approximate the biology of pot-grown plants than standard gel-based media. Shoot weight and primary root length were significantly reduced for gel-grown plants compared to rhizotron- or pot-grown plants suggesting significant differences in the biology of plants grown under these conditions (Figure 1-figure supplement 1B-C). While the 2 mm depth of the soil sheet is 10 to 20 times the average diameter of an Arabidopsis root (between 100-200 microns¹¹), we evaluated whether rhizotron-grown plants exhibited any obvious stress as a consequence of physical constriction. We compared traits of plants growing in vessels that hold similar volumes of soil but in different volumetric shapes. The number of lateral roots was significantly lower in pot and cylinder-grown plants compared to rhizotron-grown plants (Figure 1-figure supplement 1D) whereas primary root length of rhizotron and cylinder-grown plants was significantly greater than pot-grown plants (Figure 1-figure supplement 1E). No significant differences in shoot area were observed between the three systems (Figure 1-figure supplement 1-data). Thus, these data do not support the hypothesis that rhizotron-grown plants experience physical constriction greater than other vessels holding the same volume of soil.

Generation of transgenic plants expressing different luciferases Arabidopsis roots cannot easily be distinguished from soil using brightfield imaging due to their thinness and translucency (Figure 1-figure supplement 3); thus, reporter genes are needed to enhance the

183 contrast between the root and their environment. Luciferase is an ideal reporter to visualize
184 roots: 1) unlike fluorescent reporters, luciferase does not require high-intensity excitation
185 light, which could influence root growth, 2) peat-based soil (a type of histosol) exhibits no
186 autoluminescence but does autofluoresce at certain excitation wavelengths similar to GFP
187 (Figure 1-figure supplement 3), 3) while GFP is very stable, and thus not as suitable for
188 imaging dynamic transcriptional events, the luciferase enzyme is inactivated after catabolism
189 of luciferin, making it ideal for studying processes such as environmental responses. A
190 considerable number of luciferases have been developed that emit light spanning different
191 regions of the visible spectrum, but their utilization has been limited to studies in animals
192 (Table 1).

193 To determine the efficacy of using luciferase to visualize roots in soil, we codon optimized
194 sequences of *PpyRE8*, *CBGRed*, *LUC2*, and *CBG99* for Arabidopsis expression. In addition,
195 nanoLUC and venus-LUC¹² were utilized. Constitutive luciferase expression was driven
196 in plants using the *UBIQUITIN 10* (*UBQ10*) or *ACTIN2* (*ACT2*) promoters using vectors
197 assembled through a Golden-Gate cloning system¹³. Plants homozygous for a single locus
198 T-DNA insertion were evaluated for in vivo emission spectra and luminescence intensity
199 (Fig 1D). All the evaluated luciferases use D-luciferin as a substrate facilitating the simulta-
200 neous imaging of different luciferases except nanoLUC, which uses a proprietary substrate
201 furimazine¹⁴. In general, luciferases with red-shifted emission spectra were less intense than
202 the green-shifted luciferases (Fig 1D). LUC2o showed an emission maximum at 580 nm and
203 a minor peak at 620 nm while CBG99o lacks the minor peak.

204 Continuous addition of luciferin did not have any significant effect on shoot weight or primary
205 root length (Figure 1-figure supplement 4). After luciferin addition, luminescence signal
206 could be reliably detected in root systems for up to 10 days, depending on the developmental
207 state of the plant.

208 **GLO1: a semi-automated luminescence imaging system for rhizotrons** Lumines-
209 cence imaging systems commercially available for biomedical research are usually optimized

for imaging horizontally held specimens or samples in microtiter plates. Placing rhizotrons in this position would induce a gravitropic response in plants. Working with Bioimaging Solutions (San Diego, CA) we designed and built a luminescence imaging system optimized for rhizotron-grown plants. GLO1 (Growth and Luminescence Observatory 1) uses two back-thinned CCD cameras (Princeton Instruments, USA) to capture partially-overlapping images of rhizotrons while a motorized stage automatically rotates the rhizotron to capture images of both sides (Fig 1E). A composite image is generated from the images captured of each side; Fig 1F shows that approximately half of the root system is revealed on each side with few roots being visible on both sides. Apparently, the soil sheet is thick enough to block portions of the root system but thin enough to ensure its continuous structure can be compiled from opposite face views. We tested the ability of GLO1-generated images to reveal complete root systems by manually quantifying the number of lateral roots in excavated root systems of 8 different plants and testing these results against estimates of lateral root number from images of the same plants visually inspected by 4 different persons. These comparisons revealed good correlation ($(R^2 = 0.974)$) between actual lateral root counts and image-based estimation, indicating GLO1-generated root images provide an accurate representation of the in soil root system.

GLO-RIA: GLO-Roots Image Analysis We developed a set of image analysis algorithms that were well suited for the complex root systems that GLO-Roots is able to capture. GLO-RIA (Growth and Luminescence Observatory Root Image Analysis) is an ImageJ plugin divided in two modules. The first module (RootSystem) performs four different types of analysis: i) a local analysis that detects all root particles in the image and computes their position, length and direction; ii) the global analysis performs a root system level analysis and computes the total visible surface, convex hull, width and depth; iii) the shape analysis uses Elliptic Fourier Descriptors or pseudo-landmarks similarly to RootScape¹⁵ to perform a shape analysis on the root system iv) the directionality analysis computes the mean direction of root particles in a root system (either on the full image or by a user-defined region of interest in the image). These four analysis methods are fully automated by default, but

238 can be manually adjusted if needed. The second module of GLO-RIA (RootReporter) was
239 specifically designed for the analysis of multi-layered images such as combinations of gene
240 reporter, root structure and soil moisture. Shortly, the plugin works as follows: i) detection
241 of the gene reporters and the structure reporters in their respective images; ii) if needed, a
242 manual correction can be performed to correct the automated detection; iii) gene reporters
243 are linked with the soil water content and the structure reporters, based on their proximity;
244 iv) gene reporter intensity (either absolute or normalized using the structural reporter) is
245 computed; v) all data are exported and saved to a RSML datafile¹⁶. Gene and structure
246 reporters can be followed across different time and space points. Using an object oriented
247 approach, great care has been taken to facilitate the user interactions on the different images
248 to streamline the analysis process. Table 2 shows a list of root system features extracted
249 using GLO-RIA. GLO-RIA does not currently have the ability to reconstruct the root archi-
250 tecture in itself (topological links between roots). This is a challenge for analyzing images
251 captured by GLO-Roots since soil particles cause disruption of root segments.

252 We validated the measurements obtained with GLO-RIA using two approaches. First, we
253 compared the root system width, depth and individual lateral root angles of an indepent
254 set of images corresponding to different Arabidopsis accesions growing in control conditions
255 with the the width, depth and root system directionality obtained with GLO_RIA.
256 Since the root system width and depth can be manually corrected in GLO-RIA we obtained
257 almost perfect correlation for this measurements (Figure 1-figure supplement 5A,B). We also
258 obtained good correlations for the directionality and the mean lateral root angles measured
259 by GLO-RIA (Figure 1-figure supplement 5C), showing that the directionality is a good
260 estimator of the mean lateral root angle of a root system. We then used ArchiSimple¹⁷ to
261 generate 1240 images with contrasting sizes and lateral root angles. Since the images are
262 generated by the model, we can obtain very precise ground truth measurements that we
263 then used to validate the GLO-RIA obtained values for the same parameters (depth, width
264 and directionality). Again, we obtained good correlations for all three measured parameters
265 (Figure 1-figure supplement 5D-F). Sample images of the real root systems and ArchiSimple
266 generated images together with GLO-RIA directionality color-coded images are also shown

267 in (Figure 1-figure supplement 5G-I)

268 **Continuous imaging of root growth**

269 The size of our rhizotrons enables undisturbed root system development (before roots reach
270 the sides or the bottom of the rhizotron) for about 21-23 days for the Col-0 accession
271 growing under long day conditions (Figure 2); however root traits such as directionality
272 can be observed through later stages of plant development. See 35 DAS root system and
273 directionality in Figure 2A-B. An example of a time series spanning 11 to 21 days after
274 sowing (DAS) of Col-0 roots expressing *ProUBQ10:LUC2o* is shown in Fig 2A and [Video 1](#)
275 with a color-coded time projection shown in Fig 2C. Directionality analysis (Fig 2B) shows
276 a progressive change in root system angles from 0 ° (vertical) to 45 ° as lateral roots take
277 over as the predominant root type. Figure 2D shows the evolution over time of several root
278 traits that can be automatically captured by GLO-RIA (depth, width, area) and others that
279 were manually quantified (primary root growth rate or number of lateral roots per primary
280 root).

281 #### Root system architecture of different *Arabidopsis* accessions.

282 As a proof of concept to estimate the utility of our root imaging system to phenotype
283 adult root system traits, we transformed a small set of accessions (Bay-0, Col-0 and Sha)
284 with the *ProUBQ10:LUC2o* reporter and quantified RSA at 22 DAS (Fig 3A-C). GLO-RIA
285 analysis of these root systems identified several root traits that distinguish Col-0, Bay-0
286 and Sha. Directionality analysis revealed an abundance of steep-angle regions in the root
287 system of Bay while Sha showed an abundance of shallow-angled regions and Col-0 was
288 intermediate (Fig 3D). Bay-0 shows the deepest and narrowest root system leading to the
289 highest depth/width ratio while Sha has the widest root system (Fig 3E). Other root traits
290 such as root system area and the vertical center of mass also showed significant differences
291 (Figure 3-figure supplement 1B). Broad sense heritability values for depth (96.3), area (92.0),
292 depth/width (97.8), width (95.7) and vertical center of mass (95.0) were all higher than 90%.
293 To capture the richness of root architecture shape, we used GLO-RIA to extract pseudo-

294 landmarks describing the shape of the root system (see Materials and Methods for more
295 details) and performed PCA analysis. The first principal component captures differences
296 in the distribution of widths along the vertical axis and separates Col-0 and Sha from Bay-
297 0 root systems. (Fig 3F). Bay-0 shows an homogenous distribution of widths along the
298 vertical axis while Sha and Col-0 are much wider at the top than bottom. PC2 seems to be
299 capturing a relationship between width at the top and total depth and separates Sha root
300 systems which are wide at the top and deep from Col-0 root systems which are wide but
301 not as deep as Sha. Shape information extracted from pseudo-landmarks can distinguish
302 the three different accession using PCA analysis (Fig 3G)

303 **Spectrally distinct luciferases enable gene expression patterns, characterization**
304 **of root system interactions and microbial colonization.**

305 We tested whether spectrally distinct luciferase reporters would enable additional informa-
306 tion besides root architecture to be captured from root systems. Luciferase reporters have
307 been commonly used to study gene expression and these resources can potentially be utilized
308 to study such regulatory events in soil-grown roots. We transformed *ProACT2:PpyRE8o*
309 into two well studied LUC reporter lines: the auxin response reporter line *ProDR5:LUC*¹⁸
310 (Figure A-B) and the Reactive Oxygen Species (ROS) response reporter *ProZAT12:LUC*¹⁹
311 (Figure 4C-D). We implemented in GLO-RIA an algorithm that semi-automatically iden-
312 tifies gene reporter signal and associates this object to the corresponding root structure
313 segment. A graphical representation of the results obtained with Root Reporter can be
314 observed in Figure 4-figure supplement 1. Reporter intensity values along the first 5 mm
315 of root tips can also be observed in Figure 4-figure supplement 2. We then took advantage
316 of our ability to constitutively express two spectrally different luciferases and imaged the
317 overlapping root systems (one expressing *ProUBQ10:LUC2o* and the other *ProACT2:PPy*
318 *RE8o*). While two root systems were distinguishable using this system (Figure 4-figure sup-
319 plement 3); measurements of root system area did not reveal a significant effect on root
320 growth when two plants were grown in the same rhizotron, compared to one; however, fur-

³²¹ ther studies are warranted (Figure 4-figure supplement 3).
³²² The GLO-Roots system uses non-sterile growth conditions, which allows complex biotic
³²³ interactions that may affect responses to the environment. Bacteria themselves can be en-
³²⁴ gineered to express luminescent reporters through integration of the LUX operon, which
³²⁵ results in luminescence in the blue region of the spectrum and is thus compatible with
³²⁶ the plant-expressed luciferase isoforms we have tested. *Pseudomonas fluorescens* CH267²⁰,
³²⁷ a natural *Arabidopsis* root commensal, was transformed with the bacterial LUX operon
³²⁸ and used to inoculate plants. Thirteen days after inoculation, we were able to observe
³²⁹ bacterial luminescence colocalizing with plant roots. *P. fluorescens* did not show an ob-
³³⁰ vious pattern of colonization at the root system scale level. As a proof-of-principle test
³³¹ of the multi-dimensional capabilities of the GLO-Roots system we visualized both *LUC2o*
³³² and *PPyRE8o* reporters in plants and the LUX reporter in bacteria in the same rhizotron
³³³ (Figure 4-figure supplement 4).

³³⁴ **Adaptive changes in root system architecture under water deprivation, phos-**
³³⁵ **phorus deficiency and light** To test the utility of the GLO-Roots system to understand
³³⁶ response of root systems to environmental stimuli we tested the effects of light and condi-
³³⁷ tions that mimic drought and nutritional deficiency. To examine the effects of light exposure
³³⁸ on the root architecture, the black shields, which normally protect the soil and roots from
³³⁹ light, were removed from the top half of the rhizotrons 10 DAS. Using directionality analysis
³⁴⁰ we detected a significant increase in the steepness of roots only in the light exposed region of
³⁴¹ the rhizotron, while the lower shielded region showed no difference. (Fig 6-figure supplement
³⁴² 3A-B and Fig 6-figure supplement 4). Light can penetrate the top layers of soil²¹ and it
³⁴³ has been proposed to have a role in directing root growth specially in dry soils²² through
³⁴⁴ the blue light receptor *phot1*. Root directionality was not significantly different between
³⁴⁵ light and dark-treated roots of the *phot1/2* double mutant suggesting that blue light per-
³⁴⁶ ception is necessary for this response^{22,23} (Fig 6-figure supplement 3B-lower panel). These
³⁴⁷ data highlight the strong effects of light on root system architecture²⁴, which GLO-Roots
³⁴⁸ rhizotrons are able to mitigate.

349 Plants grown in low-P soil showed a significant increase in the width-depth ratio of the root
350 system compared to plants grown in P-replete soil, as determined using the automated root
351 system area finder in GLO-RIA (Fig 6-figure supplement 2A-B). Plants under P deficiency
352 showed an increase in the ratio between root-shoot area (Fig 6-figure supplement 2C) and
353 higher investment of resources in the development of the root system at the expense of shoot
354 growth (Fig 6-figure supplement 2D). Root systems of control and P-deficient plants showed
355 no significant differences in directionality at 22 DAS but at 27 DAS, roots were more hori-
356 zontally oriented in P-deficient plants (Fig 6-figure supplement 2E). The observed changes in
357 root architecture are consistent with root system ideotypes that improve phosphorus uptake
358 efficiency.

359 GLO-Roots is especially well suited for studying water-deficit (WD) responses. First, shoots
360 are exposed to the atmosphere and vapor pressure deficit (VPD) is maintained at levels that
361 allow for transpiration of water from the shoot. Second, soil in rhizotrons is exposed to air
362 at the top and dries basipetally (from the top-down); drying soil increases the volume
363 occupied by air and reduces contact of root with liquid water, all of which are similar to
364 changes in soil expected in the field during WD. Finally, as peat-based soil dries, its optical
365 properties change, allowing moisture content to be approximated from bright-field images.
366 We took advantage of the change in gray-scale pixel intensity to construct a calibration
367 curve (Figure 5-figure supplement 1) that quantitatively relates gray-scale pixel intensity to
368 moisture content (Fig 5A); water content can be color coded in images with appropriate
369 look up tables (Fig 5B). Soil color was not affected by the presence or absence of roots
370 (Figure 5-figure supplement 2). Using this approach, water content in a rhizotron can be
371 mapped and visualized in 2D (Fig 5C-D). In the example shown, we can observe that a 22
372 DAS Bay-0 plant depleted soil-moisture content locally around the the root system (Figure
373 5E).

374 We performed several trials to simulate WD in our growth system. Plants were germinated,
375 grown under control conditions then transferred to 29°C and standing water removed from
376 the container holding the rhizotrons starting at 9 DAS or 13 DAS. Elevated temperature

377 combined with water deficit is a common stress that modern crops varieties are poorly
378 adapted to, thus highlighting the importance of examining this combined treatment^{25,26}.
379 Plants were maintained in this WD regime until 22 DAS when luciferin solution was added
380 and the plants imaged. At 13 DAS, lateral roots near the soil surface are already emerged
381 ([Video 1](#), Figure 2A) and 9 days of subsequent WD treatment caused lateral roots to show an
382 increase in gravitropism leading to the development of a root system that were deeper and
383 more vertically oriented (Fig 6A). Roots of Bay-0 plants showed similar responses, though
384 the extent of change was less pronounced since Bay-0 roots are normally more vertically
385 oriented (Fig 6B). Plants transferred at 9 DAS and grown for 13 days under WD showed
386 less lateral root development in the top layer of soil (Fig 6E). At this time point, lateral roots
387 start to emerge ([Video 1](#)) and early drought may lead to growth quiescence or senescence.
388 Careful examination of roots in these regions showed evidence of small lateral root primordia
389 populating the primary root (Figure 6F). After 24 h of re-watering (Figure 6G) these lateral
390 root primordia reinitiated growth (Figure 6H).

391 Time-lapse imaging of the water deficit response showed that changes in root growth direc-
392 tion occurred ahead of the dry soil front [Video 2](#). Using GLO-RIA we were able correlate
393 local water moisture contents with the orientation of root segments. With this approach we
394 observed that root segments in dryer areas of rhizotron grew at steeper root angles (Figure
395 7) than roots in WW regions, though lateral root angle in wetter regions was also affected.
396 These data suggest that both local and systemic signaling is likely involved in redirecting
397 lateral roots deeper during the simulated drought treatments tested here.

398 We also grew plants under WD at control temperatures or under WW conditions at elevated
399 temperature to test the effects of these individual stresses on root architecture. We observed
400 that both conditions were sufficient to induce a change in root directionality indicating that
401 the plant uses similar mechanisms to avoid heat and water-deficit associated stresses (Figure
402 6-figure supplement 1). We next asked which regulatory pathways controlled the observed
403 changes in lateral root directionality during simulated drought. Hydrotropism is a known
404 environmental response that directs root growth towards wet regions of soil. MIZ1 is an

405 essential regulator of hydrotropism; however *miz1* mutants had no significant effect on water
406 deficit-induced changes in root directionality, compared to wild type (Fig 6C), indicating
407 that this response was distinct from hydrotropism. Auxin is an important mediator of
408 gravitropism and auxin treatment causes lateral roots to grow more vertically⁷. Consistent
409 with this role for auxin, mutant plants with loss of function in the auxin receptor TIR1, did
410 not show changes in the root system directionality between WW and WD conditions (Fig
411 6D).

412 **GLO-Roots for Brachypodium and Tomato.**

413 To examine the general applicability of the GLO-Roots system for other species, we intro-
414 duced LUC2o-expressing reporters into the model grass *Brachypodium distachyon* and the
415 crop plant *Lycopersicon esculentum* (tomato). Brachypodium is well suited to the GLO-Root
416 system because, like Arabidopsis, its small size allows mature root systems to be studied in
417 relatively small soil volumes^{27,28}. *LUC2o* driven by the *ZmUb1* promoter was introduced into
418 Brachypodium using the pANIC vector²⁹. Brachypodium roots showed a distinct architec-
419 ture from Arabidopsis marked by prolific development of secondary and tertiary lateral roots
420 (Fig 8A). This is consistent with other studies that show that Brachypodium has a typical
421 grass root system²⁸. Comparison of root system development in rhizotrons with gel-based
422 media showed that root growth is higher in soil than in plates (Figure 8-figure supplement
423 1). Previous work has suggested that auxin levels in Brachypodium roots is sub-optimal for
424 growth³⁰. Pacheco-Villalobos and colleagues suggest that, in Brachypodium, and contrary
425 to what happens in Arabidopsis, ethylene represses *YUCCA* reducing the synthesis of auxin.
426 The reduced growth that we observe in plates and the high levels of ethylene that build up
427 in sealed plates³¹ would support this mechanism.

428 Tomato plants were transformed with *Pro35S:PPyRE8o* and *ProeDR5rev:LUC2* reporters.
429 The plants showed more rapid growth than Arabidopsis or Brachypodium and required
430 fertilizer to prevent obvious signs of stress (reduced growth, anthocyanin accumulation).
431 Root systems were imaged from 17 DAS plants. Roots showed presumptive lateral root

432 primordia marked by DR5-expression (Fig 8C-D). These results show that the GLO-Roots
433 method can be applied to study root systems of plants and will likely be useful for studying
434 root systems of other small to medium sized model plants and for early stages of larger crop
435 plants.

436 **Discussion**

437 **GLO-Roots enables a multi-dimensional understanding of root biology**

438 Recent studies of root systems has emphasized structural attributes as important contrib-
439 utors of root system function. Indeed, studies examining the role of genetic variants in
440 tolerating abiotic stress have demonstrated the importance of such characteristics⁸. Roots,
441 however, are highly diverse in the biology they perform and a multi-dimensional understand-
442 ing of root systems, which incorporates differences in signaling, metabolism and microbial
443 association as well as structure, may provide a clearer understanding of the degree to which
444 sub-functionalization of the root system plays a role in important processes such as acclima-
445 tion and efficient resource acquisition.

446 We have developed tools in GLO-Roots that allow for tracking multiple aspects of soil
447 physicochemical properties and root biology simultaneously. Using GLO-Roots, we are able
448 to map in 2D coordinates soil physical properties such soil moisture together with root ar-
449 chitecture traits such as directionality, growth rates and gene expression levels. All this
450 information is aggregated in layers for each x, y coordinate. Using GLO-RIA we integrate
451 this multilayer information, leveraging our ability to simultaneously and seamlessly inves-
452 tigate root responses to environmental stimuli such as soil moisture content. Luciferase
453 isoforms that emit light at different wavelengths allow for constitutive and regulated pro-
454 moters to be studied together. Introduction of luciferase reporters into microbes provides
455 an additional layer of information that provides a readout on the association between or-
456 ganisms and how this might be affected by environmental conditions. The flexibility of the
457 GLO-Roots system may enable additional dimensionality to our understanding of root biol-

ogy. Other physical properties such as CO₂ or pH mapping in rhizotrons have already been enabled by using planar optodes³². It may be possible to engineer LUX-based reporters in microbes that are responsive to extracellular metabolites, creating microbial biosensors, and integration of such tools may enable root-exudation and nutrition to be analyzed in soil. Split-Luciferase reporters have been engineered that allow bi-molecular interactions to be studied. Finally, molecular sensors analogous to FRET sensors, termed BRET-sensors³³, may allow metabolite tracking dynamically through the root system. With additional innovation in the development of luciferase reporters, the GLO-Roots systems will likely expand the repertoire of biological processes that can be studied over an expanded range of developmental time points and environmental conditions.

Enhanced root growth and gravitropism may constitute an avoidance mechanism used during water deficit stress

It has been proposed that plants with steep root systems will be better able to tap into deep water resources and thus perform better under water deprivation. For example in rice, the IR64 paddy cultivar shows shallow root systems in upland fields whereas Kinandang Patong, an upland cultivar, is deeper rooting⁸. Plants maintain a number of regulatory pathways that mediate changes in physiology during WD. Enhanced growth of root systems has been well characterized in field-grown plants; however this has not been recapitulated in studies of gel-grown *Arabidopsis* plants. Thus, it has been unclear whether *Arabidopsis* simply responds to WD differently. Our results here show that *Arabidopsis* does indeed maintain a classical WD response that expands the root system and directs growth downward. Interestingly, under our stress regime, we did not observe a significant decrease in the relative water content of shoot tissues (Figure 6-figure supplement 5), suggesting that the changes in root architecture were sufficient to provide access to deep water and prevent dehydration. Such changes in root growth are likely regulated through systemic and local signaling that involve auxin signaling but acts independently of known pathways that control moisture-directed root growth.

485 **Perspectives and Conclusions**

486 Understanding plant biology requires a sophisticated understanding of how environmental
487 stimuli affect the form and function of plants as well as an understanding of how physiological
488 context informs such responses. Environmental conditions are at least as complex as the
489 plants they affect. Plant roots are exposed to a variety of environmental signals that change
490 in time and space at very different scales that are integrated at the whole plant system. It is
491 an important challenge in biology to develop methods of growing and studying plants that
492 present such stimuli in a manner that the plant is likely to encounter in nature. After all, the
493 plants we study have evolved to survive through mechanisms that have been selected, over
494 evolutionary time, in nature. It will be interesting for future studies to determine how other
495 environmental stimuli affect root growth using GLO-Roots and whether these responses
496 differ between accessions of Arabidopsis. Identification of the genetic loci responsible for
497 phenotypic variation in adult root phenotypes may identify the molecular basis for adaptive
498 variation that exists in this species and potentially identify loci that are useful for breeding
499 efforts needed for the next green revolution.

500 **Materials and methods**

501 **Growth system**

502 **Rhizotrons and growth system fabrication.** Rhizotrons are composed of two sheets of
503 1/8" abrasion resistant polycarbonate plastic (Makrolon AR (R)) cut to size using a water
504 jet (AquaJet LLC, Salem, OR), two acrylic spacers cut using a laser (Stanford Product
505 Realization Lab), two rubber U-channels cut to strips 30 cm long ([McMaster Carr part](#)
506 [# 8507K33](#)) and two sheets of black 0.030" thick polypropylene sheets ([McMaster Carr](#)
507 [part # 1451T21](#)) cut with a straight-edge razor blade. Rhizotron designs were drafted in
508 Adobe Illustrator (Adobe, San José, CA). The blueprints of all the parts are provided in
509 Supplement 1. The top edge of each polycarbonate sheet was painted with black 270 Stiletto
510 nail polish (Revlon, New York, NY).

511 **Boxes and holders.** Rhizotrons are held vertical during plant growth in a custom rack sys-
512 tem composed of two sheets of 1/4" black acrylic plastic cut with slots for eleven rhizotrons
513 using a laser, four 3/8" PVC rods ([McMaster Carr part # 98871a041](#)) secured with PVC
514 nuts ([McMaster Carr part # 94806a031](#)) to hold the acrylic sheets horizontal. The rack is
515 placed inside a 12" x 12" x 12" black polyethylene tank ([Plastic Mart part # R121212A](#)).

516 **Rhizotron preparation** The procedure to construct a rhizotron with soil is as follows:
517 Two pieces of polycarbonate plastic are laid flat on a table with the spacers inserted. Using
518 an electric paint gun, a fine mist of water is applied to the bare polycarbonate sheets. Then,
519 using a 2 mm sieve (US Standard Sieve Series N° 10) a fine layer of PRO-MIX(r) PGX soil
520 (Premier Tech, Canada) is applied. Excess soil is discarded by gently tapping the plastic
521 against the table in a vertical position. Water is sprayed again onto the soil, then a second
522 layer of Pro-MIX is applied as before. For P deficiency experiments soil supplemented with
523 1 ml of 100 µM P-Alumina (control) and 0-P-Alumina (P deficient) was used. To prevent
524 the soil from falling out of the bottom opening, a 3 x 6 cm piece of nylon mesh is rolled into
525 a 1 cm wide tube and placed at the bottom side of the rhizotron. The spacers are removed
526 and replaced by clean spacers. The two faces of the rhizotron are carefully joined together
527 and two rubber U-channels slipped on to clamp all pieces together. Assembled rhizotrons
528 are placed into the rack inside the boxes and 500 mL of water is added to the box.

529 **Plant growth** *Arabidopsis thaliana* seeds were stratified for 2 d at 4 °C in Eppendorf tubes
530 with distilled water. Seeds were suspended in 0.1 % agar and 5 to 10 were sown using
531 a transfer pipette in the rhizotron. A transparent acrylic sheet was mounted on top of
532 the box and sealed with tape to ensure high humidity conditions that enable *Arabidopsis*
533 germination. Three days after sowing, the cover was unsealed to decrease humidity and
534 allow the seedlings to acclimate to a dryer environment. From 3 days after sowing (DAS)
535 to the time the first true leaves emerged, it was critical to ensure that the top part of the
536 rhizotron remained humid for proper germination of the plants. Between three and five DAS
537 the rhizotrons were thinned leaving only the number plants required for that experiment,
538 typically one, except for experiments examining root-root interactions. Unless otherwise

539 stated, all the experiments presented here, treatments were started 10 DAS. Plants were
540 grown under long day conditions (16 h light / 8 h dark) using 20–22 °C (day/night) and
541 150 µE m⁻¹ s⁻¹. Two types of growth environments were used for experiments. A walk-in
542 growth chamber with fluorescent lightning and a growth cabinet with white LED lights.
543 Relative water content measurements were done as previously described³⁴

544 **qRT-PCR analysis.**

545 Seeds were surface sterilized as described before² and grown in rhizotrons, 100 cm³ pots, or
546 on two types of 1% agar (Duchefa) media containing either 1x MS nutrients (Caisson) and 1%
547 Sucrose, (termed ms media) or ¼x MS nutrients only (termed ms25 media). Both media were
548 buffered using 0.5 g/L MES and pH was adjusted to 5.7 with KOH. All plants were grown
549 together in a growth cabinet with LED lights under long day conditions (16h day/8h night).
550 Root and shoot tissue was collected separately from individual plants at the end of the day
551 (1 hour before the lights shut off) and at the end of the night (1 hour before lights came on).
552 Three biological replicates were collected for each condition. RNA was extracted using the
553 Plant RNA MiniPrepTM kit (ZYMO Research) according to manufacturer's instructions
554 with on-column DNase treatment (Qiagen). cDNA was made using the iScript Advanced
555 cDNA Synthesis for RT-qPCR kit (Bio-Rad) from 200 ng of total RNA. qRT-PCR was
556 performed using a Fluidigm BioMarkTM 96.96 Dynamic Array IFC with the EvaGreen®
557 (Bio-Rad) fluorescence probe according to the Fluidigm Advanced Development Protocol
558 number 37. For the analysis, all the reactions with no amplification ($C_t = 999$) were set to
559 the maximal C_t for that assay type. The two technical replicates were then averaged and
560 dC_t values calculated using AT3G07480, AT4G37830, At1g13320 and At1g13440 as reference
561 internal controls. PCA plots were generated with Devium Web³⁵ using dC_t values. dCT
562 values were calculated as $dCT = CT_{\text{gene interest}} - \text{mean}(CT_{\text{reference gene}})$. Primers
563 used are listed in file Supplement 8.

564 **Biological components**

565 **Codon optimization of luciferases.** The following luciferases that emit light at different
566 wavelengths were codon optimized for Arabidopsis (Genscript, Piscataway, NJ): LUC2: a
567 yellow improved version (Promega, Madison, WI) of the original *Photinus pyralis* (firefly)
568 LUC.

- 569 • Ppy RE8: a red variant³⁶ of the *P. pyralis* thermostable variant Ppy RE-TS³⁷.
- 570 • CBG99: a green variant (Promega, Madison, WI) from yellow click beetle (*Pyrophorus*
571 *plagiophthalmus*) luciferases.
- 572 • CBR: a red variant (Promega, Madison, WI) from yellow click beetle.

573 **Non-optimized luciferases.** We also used the following non-optimized luciferases:

- 574 • nanoLUC: a blue luciferase isolated from a deep sea shrimp¹⁴.
- 575 • venusLUC2: a venus-LUC2 fusion reported to show higher luminescence output than
576 LUC2¹².
- 577 • A transposon containing the bacterial luciferase-containing LUX operon was inte-
578 grated into the *Pseudomonas fluorescens* CH267²⁰ genome by conjugation with *E.*
579 *coli* SM10 *pir* containing pUT-EM7-LUX³⁸ and used to track root microbe coloniza-
580 tion. For inoculation 9 DAS plants were inoculated with 2 mL of an overnight bacterial
581 culture resuspended in 10 mM MgSO₄ and diluted to 0.01 OD.

582 **Generation of single-reporter transgenic plants.** We generated transcriptional fu-
583 sions of all luciferases to constitutive promoters to examine the activity level and emission
584 spectrum of each isoform. The *attL1-attL2* entry clones containing plant-codon optimized
585 coding sequence of *LUC2*, *PpyRe8*, *CBG99* and *CBR* were synthesized by Genscript. A
586 DNA fragment including the *UBQ10* promoter region and first intron was amplified from
587 Col-0 genomic DNA with primers incorporating the attB1, attB4 combination sites at the 5'

and 3' respectively. The PCR product was then introduced into pDONR™ P4-P1R (Invitrogen) through a classic Gateway BP-reaction. The resulting plasmid, the *attL1-attL2* entry clones with luciferase sequences, an empty *attR2-attL3** entry clone and the destination vector dpGreenmCherry² were used to construct *ProUBQ10:LUC2o*, *ProUBQ10:PpyRE8o*, *ProUBQ10:CBG99o* and *ProUBQ10:CBRo* through Gateway LR reactions. The destination vector *dpGreenmCherry* contains a plasma membrane-localized mCherry coding sequence driven by the 35S promoter and is used as a selectable marker of transformation at the mature seed stage². We used Golden Gate cloning and the destination vectors that we had generated before¹³ for the following fusions: *ProUBQ10:nanoLUC2*, *ProUBQ10:venusLUC*, *ProACT2:PpyRE8o*. Briefly, the different components of each construct were PCR amplified with complementary BsaI or SapI cutting sites, mixed with the destination vector in a single tube, digested with either BsaI or SapI, ligated with T4 DNA ligase, then transformed into *E. coli* Top10 cells and plated on LB antibiotic plates containing X-gal as previously described¹³. Junction sites were confirmed by sequencing. We used pSE7 (Addgene ID #: pGoldenGate-SE7: 47676) as the destination vector of the *ProUBQ10:nanoLUC2*, *ProUBQ10:venusLUC* constructs and pMYC2 (Addgene ID #: pGoldenGate-MCY2: 47679) as the destination vector for *ProACT2:PpyRE8o*. Maps of all the vectors can be found in Supplement 8. *ProUBQ10:LUC2o* was transformed into Col-0, Bay and Sha accessions, the *tir1-1*³⁹ mutant and the *miz1*⁴⁰ T-DNA insertion line (SALK_126928).

Brachypodium distachyon The *Arabidopsis* plant-codon optimized Luciferase gene, *LUC2o*, was inserted into the monocot vector pANIC10 via Gateway cloning²⁹. *Brachypodium distachyon* plants were transformed using the method of Vogel and Hill⁴¹.

Tomato The transcriptional fusion *ProeDR5:LUC2* was generated by cloning the *ProeDR5:LUC2* DNA fragment into the pBIB expression vector via restriction sites SalI and Acc65I. The eDR5 promoter is an enhanced version of DR5 containing 13 repeats of the 11-nucleotide core DR5 element⁴² and the pBIB expression vector contains an NPTII resistance gene under the control of the NOS promoter for use as a selectable marker during

615 transformation. All tomato transformations were performed by the Ralph M. Parsons
616 Foundation Plant Transformation Facility (University of California, Davis).

617 **Generation of dual-reporter plants.** To generate dual-reporter plants expressing lu-
618 ciferase isoforms that emit light with divergent emission spectra we used *ProACT2:PpyRE8o*
619 as the root structural marker and ZAT12:LUC¹⁹ and DR5:LUC+¹⁸ lines that were trans-
620 formed with the *ProACT2:PpyRE8o* construct. All constructs were transformed using a
621 modified floral dip method as described in².

622 To make the dual color tomato plants, the *Pro35S:PpyRE8o* transcriptional fusion was
623 generated by putting the plant-codon optimized coding sequence described above into the
624 pMDC32 expression vector through a Gateway LR reaction. The pMDC32 vector con-
625 tains a hygromycin resistance gene under the control of the 35S promoter for use as a se-
626 lectable marker during transformation. This construct was transformed into the transgenic
627 *ProeDR5:LUC2* tomato line.

628 **In vivo emission spectra of plants constitutively expressing luciferase isoforms.**
629 To generate *in vivo* emission spectra of all constitutively expressed luciferases, seeds were
630 sterilized and sown on MS plates as described before². After 8 days, seedlings were treated
631 with a 100 µM luciferin solution, incubated at room temperature for 3 hours and imaged
632 using an IVIS Spectrum imaging system (Perkin Elmer, Waltham , MA) using 20 nm band-
633 pass emission filters at the following wavelengths (in nm: 490-510, 510-530, 530-550, 550-570,
634 570-590, 590-610, 610-630, 630-650, 650-670, 670-690, 690-710). Raw images were analyzed
635 using Fiji and *in vivo* emission spectra were constructed. The full emission spectra of LUX
636 and nanoLUC could not be constructed since the maximum of these two luciferases is below
637 the lower band pass filter that were available.

638 **Imaging system** We designed a custom imaging system (GLO1, Growth and Lumines-
639 cence Observatory 1) optimized for imaging dual-reporter luciferase expression in our custom
640 rhizotrons. The design was a joint effort with Bioimaging Solutions (San Diego, CA) who

641 also built the system and wrote the acquisition software that drives all the mechanical parts
642 of the system. The system is composed by two 2048 x 2048 PIXIS-XB cameras (Princeton
643 Instruments, Trenton, NJ) mounted on top of each other to capture two fields of view en-
644 compassing approximately two 15 x 15 cm areas corresponding to the top or bottom of the
645 rhizotron. The cameras are fitted with a Carl-Zeiss macro lens. A filter wheel with space
646 for four, 76.2 mm filters is positioned in front of the cameras and controlled by a stepper
647 motor allowing for automated changing of the filter wheel position. We used two -542/50
648 and 450/70- custom cut Brightline(R) band-pass filters (Semrock, Rochester, NY). In sin-
649 gle color imaging mode, the filter wheel is operated without filters. Positioned in front of
650 the filter wheel is a removable rhizotron holder mounted on a stepper motor. This stepper
651 motor is also controlled by the GLO-1 software allowing automatic acquisition of images
652 from both sides of the rhizotron sequentially. The whole imaging system is enclosed in a
653 light-tight black box with a door that allows loading and un-loading of rhizotrons.

654 **Plant Imaging** Around 50 mL of 300 μ M D-luciferin (Biosynth, Itasca, IL) was added to
655 soil at the top of the rhizotron. In general 5 min exposures were taken per rhizotron, per
656 side, per channel. For daily imaging experiments, plants were imaged at dawn (+/- 1 hr)
657 to reduce possible effects on diurnal rhythms of keeping plants in the dark during imaging.
658 Shoot images were taken using a Nikon D3100 camera.

659 **Image Preparation** Four individual images are collected: top front, bottom front, top
660 back and bottom back. Using an automated [ImageJ macro](#), a composite image is generated
661 as follows: 1)To correct for differences in background values between the two cameras the
662 mean background value of each image is subtracted from 200; 2) images are rotated and
663 translated to control for small misalignments between the two cameras; 3) the top and
664 bottom images of each side are merged; 4) the back image is flipped horizontally; 5) the
665 front and back images are combined using the maximum values. When dual color images are
666 acquired this operation is repeated for each channel. The final images produced are 16-bit
667 depth and 4096 x 2048 pixels. The scale of the images is 138.6 pixels per cm. Considering

668 that an Arabidopsis roots is 100 μm this results in 1.39 pixels across an Arabidopsis root.

669 **GLO-RIA imageJ plug-in** GLO-RIA uses a combination of existing tools to extract
670 relevant root architecture features. Directionality is acquired using the [directionality plugin](#)
671 from ImageJ. After the number of direction bins (we usually use bins of 2 °) is defined by the
672 user, a 5x5 sobel operator is used to derive the local gradient orientation. This orientation
673 is then used to build a distribution of directions by assigning the square of the orientation
674 into the appropriate bin. Instead of representing the total counts at each orientation a
675 relative value is calculated by dividing the individual values at each bin by the total sum
676 of the histogram (and multiplying by 100). Similar algorithms have been used to quantify
677 dynamic changes in the plant cytoskeleton⁴³.

678 The Elliptic Fourier Descriptors are aquired using the [Fourier Shape Analysis plugin](#) on
679 convex hull shape of the root system. Elliptic Fourier Descriptors have been used in numer-
680 ous studies to analyse variations in shapes, notably in leaves (e.g⁴⁴) The shape analysis is
681 inspired by RootScape¹⁵. Due to the absence of fixed, recognisable structures in root system
682 (that are required for the position of true landmarks), pseudo-landmarks are automatically
683 extracted from the root systems. Shortly, the image is divided vertically at equidistant posi-
684 tions (with the number defined by the user) and for each of the image stripes, the minimum
685 and maximum x coordinates are computed. The shape analysis is therefore able to discrim-
686 inate root system with different vertical root distributions or global root system orientation
687 (e.g. chemotropism) . The code source for the plugin, manual and sample images can be
688 found in the [github repository](#) of the project.

689 Statistical analysis was performed in R⁴⁶. The tidyR⁴⁷, dplyr⁴⁷, gridExtra⁴⁸, shapes⁴⁹,
690 geomorph⁵⁰, ggplot2⁵¹ and cowplot⁵² packages were used for data preparation, analysis
691 and plotting. Final figure preparation was done in [Inkscape](#).

692 **Data availability** All the scripts and original data used to analyze and produce the
693 images can be accessed in the Github repository of the project: github.com/rr-lab/GLO-
694 Roots. Raw files of all the images used in the paper are availabe in [Dryad](#).

695 Acknowledgements

696 Work in the lab of JRD was funded by the Carnegie Institution for Science Endowment
697 and grants from the National Science Foundation (MCB-115795) and Department of En-
698 ergy, Biological and Environmental Research program (DE-SC0008769). RRA was sup-
699 ported by a Carnegie Postdoc Fellowship and currently by Conacyt Ciencia Básica Joven
700 Investigador grant number (CB-2014-01-238101). GL was supported by the Belgian Fonds
701 de la Recherche Scientifique. JM was funded by the National Science Foundation (IOS-
702 0820854). CH is funded by MGH Toteston & Fund for Medical Discovery Fellowship grant
703 2014A051303 and NIH R37 grant GM48707 and NSF grant MCB-0519898 awarded to Fred-
704 erick Ausubel, and previously by the Gordon and Betty Moore Foundation through Grant
705 GBMF 2550.01 from the Life Sciences Research Foundation. JV was funded by the Office
706 of Biological and Environmental Research, Office of Science, US Department of Energy, in-
707 teragency agreements DE-SC0001526 and DE-AI02-07ER64452. We thank Robert Mittler
708 and Philip Benfey for providing seeds of ZAT12:LUC and DR5:LUC+ respectively. We also
709 thank Neil Robbins and members of the Dinneny lab for critical review of the manuscript
710 and suggestions during the development of the project. We greatly appreciate Tim Doyle at
711 the Stanford Small Animal Imaging Facility for providing's advice in using and help with
712 luciferase-based imaging approaches.

713 Competing interests

714 We do not have any competing interests that we are aware of.

964 **References**

- 965 1.Dinneny, J. R. *et al.* Cell identity mediates the response of *Arabidopsis* roots to abiotic
966 stress. *Science* **320**, 942–945 (2008).
- 967 2.Duan, L. *et al.* Endodermal ABA Signaling Promotes Lateral Root Quiescence during
968 Salt Stress in Arabidopsis Seedlings. *Plant Cell* **25**, 324–341 (2013).
- 969 3.Lynch, J. P. & Wojciechowski, T. Opportunities and challenges in the subsoil: pathways
970 to deeper rooted crops. *J. Exp. Bot.* **66**, 2199–2210 (2015).
- 971 4.Brady, N. C. & Weil, R. R. *Elements of the nature and properties of soils*. (Prentice Hall,
972 2009).
- 973 5.Bao, Y. *et al.* Plant roots use a patterning mechanism to position lateral root branches
974 toward available water. *Proc Natl Acad Sci* **111**, 9319–9324 (2014).
- 975 6.Tabata, R. *et al.* Perception of root-derived peptides by shoot LRR-RKs mediates systemic
976 N-demand signaling. *Science* **346**, 343–346 (2014).
- 977 7.Rosquete, M. R. *et al.* An Auxin Transport Mechanism Restricts Positive Orthogravit-
978 ropicism in Lateral Roots. *Current Biology* **23**, 817–822 (2013).
- 979 8.Uga, Y. *et al.* Control of root system architecture by DEEPER ROOTING 1 increases
980 rice yield under drought conditions. *Nat. Genet.* **45**, 1097–1102 (2013).
- 981 9.Postma, J. A. & Lynch, J. P. The optimal lateral root branching density for maize depends
982 on nitrogen and phosphorus availability. *Plant Physiol.* **166**, 590–602 (2014).
- 983 10.Schneider, C. A., Rasband, W. S. & Eliceiri, K. W. NIH Image to ImageJ: 25 years of
984 image analysis. *Nature methods* **9**, 671–675 (2012).
- 985 11.Meijon, M., Satbhai, S. B., Tsuchimatsu, T. & Busch, W. Genome-wide association study
986 using cellular traits identifies a new regulator of root development in. *Nat. Genet.* **46**, 77–81
987 (2013).
- 988 12.Hara-Miyauchi, C. *et al.* Bioluminescent system for dynamic imaging of cell and animal
989 behavior. *Biochem. Biophys. Res. Commun.* **419**, 188–193 (2012).

- 990 13.Emami, S., Yee, M.-C. & Dinneny, J. R. A robust family of Golden Gate Agrobacterium
991 vectors for plant synthetic biology. *Front. Plant Sc.* **4**, 339 (2013).
- 992 14.Hall, M. P. *et al.* Engineered Luciferase Reporter from a Deep Sea Shrimp Utilizing a
993 Novel Imidazopyrazinone Substrate. *ACS chemical biology* **7**, 1848–1857 (2012).
- 994 15.Ristova, D. *et al.* RootScape: a landmark-based system for rapid screening of root
995 architecture in Arabidopsis. *Plant Physiology* **161**, 1086–1096 (2013).
- 996 16.Lobet, G. *et al.* Root System Markup Language: toward a unified root architecture
997 description language. *Plant Physiol.* **167**, 617–627 (2015).
- 998 17.Pagès, L. *et al.* Calibration and evaluation of ArchiSimple, a simple model of root system
999 architecture. *Ecological Modelling* **290**, 76–84 (2014).
- 1000 18.Moreno-Risueno, M. A. *et al.* Oscillating gene expression determines competence for
1001 periodic *Arabidopsis* root branching. *Science* **329**, 1306–1311 (2010).
- 1002 19.Miller, G. *et al.* The plant NADPH oxidase RBOHD mediates rapid systemic signaling
1003 in response to diverse stimuli. *Science Signaling* **2**, ra45 (2009).
- 1004 20.Haney, C. H., Samuel, B. S., Bush, J. & Ausubel, F. M. Associations with rhizosphere
1005 bacteria can confer an adaptive advantage to plants. *Nature Plants* **1**, 15051 (2015).
- 1006 21.Mandoli, D. F., FORD, G. A., WALDRON, L. J., NEMSON, J. A. & Briggs, W. R. Some
1007 spectral properties of several soil types: implications for photomorphogenesis*. *Plant Cell*
1008 *Environ.* **13**, 287–294 (1990).
- 1009 22.Galen, C., Rabenold, J. J. & Liscum, E. Functional ecology of a blue light photoreceptor:
1010 effects of phototropin-1 on root growth enhance drought tolerance in *Arabidopsis thaliana*.
1011 *New Phytol.* **173**, 91–99 (2007).
- 1012 23.Moni, A., Lee, A. Y., Briggs, W. R. & Han, I. S. The blue light receptor Phototropin 1
1013 suppresses lateral root growth by controlling cell elongation. *Plant Biology* 34–40 (2014).
- 1014 24.Yokawa, K., Kagenishi, T. & Baluška, F. Root photomorphogenesis in laboratory-
1015 maintained *Arabidopsis* seedlings. *Trends Plant Sci.* **18**, 117–119 (2013).

- 1016 25.Lobell, D. B. *et al.* Greater Sensitivity to Drought Accompanies Maize Yield Increase in
1017 the U.S. Midwest. *Science* **344**, 516–519 (2014).
- 1018 26.Ort, D. R. & Long, S. P. Limits on Yields in the Corn Belt. *Science* **344**, 484–485 (2014).
- 1019 27.Pacheco-Villalobos, D. & Hardtke, C. S. Natural genetic variation of root system archi-
1020 tecture from Arabidopsis to Brachypodium: towards adaptive value. *Philosophical Trans-
1021 actions of the Royal Society of London B: Biological Sciences* **367**, 1552–1558 (2012).
- 1022 28.Watt, M., Schneebeli, K., Dong, P. & Wilson, I. W. The shoot and root growth of
1023 Brachypodium and its potential as a model for wheat and other cereal crops. *Functional
1024 Plant Biol.* **36**, 960–969 (2009).
- 1025 29.Mann, D. G. J. *et al.* Gateway-compatible vectors for high-throughput gene functional
1026 analysis in switchgrass (*Panicum virgatum L.*) and other monocot species. *Plant Biotechnol.
1027 J.* **10**, 226–236 (2012).
- 1028 30.Pacheco-Villalobos, D., Sankar, M., Ljung, K. & Hardtke, C. S. Disturbed Local
1029 Auxin Homeostasis Enhances Cellular Anisotropy and Reveals Alternative Wiring of
1030 Auxin-ethylene Crosstalk in *Brachypodium distachyon* Seminal Roots. *PLoS Genet* **9**,
1031 e1003564 (2013).
- 1032 31.Buer, C. S., Wasteneys, G. O. & Masle, J. Ethylene modulates root-wave responses in
1033 *Arabidopsis*. *Plant Physiology* **132**, 1085–1096 (2003).
- 1034 32.Blossfeld, S., Schreiber, C. M., Liebsch, G., Kuhn, A. J. & Hinsinger, P. Quantitative
1035 imaging of rhizosphere pH and CO₂ dynamics with planar optodes. *Annals of Botany* **112**,
1036 267–276 (2013).
- 1037 33.Shaw, S. L. & Ehrhardt, D. W. Smaller, Faster, Brighter: Advances in Optical Imaging
1038 of Living Plant Cells. *Annu. Rev. Plant Biol.* **64**, 351–375 (2013).
- 1039 34.Barr, H. & Weatherley, P. A re-examination of the relative turgidity technique for esti-
1040 mating water deficit in leaves. *Aust. J. Biol. Sci* **15**, 413–428 (1962).
- 1041 35.Grapov, D. DeviumWeb: Dynamic Multivariate Data Analysis and Visualization Plat-

- 1042 form.
- 1043 36.Branchini, B. R. *et al.* Red-emitting luciferases for bioluminescence reporter and imaging
1044 applications. *Analytical Biochemistry* **396**, 290–297 (2010).
- 1045 37.Branchini, B. R. *et al.* Thermostable red and green light-producing firefly luciferase
1046 mutants for bioluminescent reporter applications. *Analytical Biochemistry* **361**, 253–262
1047 (2007).
- 1048 38.Lane, M. C., Alteri, C. J., Smith, S. N. & Mobley, H. L. T. Expression of flagella is
1049 coincident with uropathogenic Escherichia coli ascension to the upper urinary tract. *Proc.
1050 Natl. Acad. Sci. U.S.A.* **104**, 16669–16674 (2007).
- 1051 39.Ruegger, M. *et al.* The TIR1 protein of Arabidopsis functions in auxin response and is
1052 related to human SKP2 and yeast grr1p. *Genes Dev* **12**, 198–207 (1998).
- 1053 40.Moriwaki, T. *et al.* Hormonal Regulation of Lateral Root Development in Arabidopsis
1054 Modulated by MIZ1 and Requirement of GNOM Activity for MIZ1 Function. *Plant Physiol.*
1055 **157**, 1209–1220 (2011).
- 1056 41.Vogel, J. & Hill, T. High-efficiency Agrobacterium-mediated transformation of Brachy-
1057 podium distachyon inbred line Bd21-3. *Plant Cell Rep* **27**, 471–478 (2008).
- 1058 42.Covington, M. F. & Harmer, S. L. The Circadian Clock Regulates Auxin Signaling and
1059 Responses in Arabidopsis. *Plos Biol* **5**, e222 (2007).
- 1060 43.Lindeboom, J. J. *et al.* A Mechanism for Reorientation of Cortical Microtubule Arrays
1061 Driven by Microtubule Severing. *Science* **342**, 1245533–1–1245533–11 (2013).
- 1062 44.Chitwood, D. H. *et al.* A modern ampelography: a genetic basis for leaf shape and
1063 venation patterning in grape. *Plant Physiology* **164**, 259–272 (2014).
- 1064 45.Iwata, H. & Ukai, Y. SHAPE: a computer program package for quantitative evaluation of
1065 biological shapes based on elliptic Fourier descriptors. *The Journal of Heredity* **93**, 384–385
1066 (2002).

- 1067 46.R Core Team. *R: A language and environment for statistical computing*. (R Foundation
1068 for Statistical Computing, 2014). at <<http://www.R-project.org/>>
- 1069 47.Wickham, H. *Tidyr: Easily tidy data with spread() and gather() functions*. (2014). at
1070 <<http://CRAN.R-project.org/package=tidyr>>
- 1071 48.Auguie, B. *GridExtra: Functions in grid graphics*. (2012). at <[http://CRAN.R-project.](http://CRAN.R-project.org/)
1072 [org/package=gridExtra](#)>
- 1073 49.Dryden, I. L. *Shapes: Statistical shape analysis*. (2013). at <[http://CRAN.R-project.](http://CRAN.R-project.org/)
1074 [org/package=shapes](#)>
- 1075 50.Adams, D. & Otarola-Castillo, E. Geomorph: An r package for the collection and analysis
1076 of geometric morphometric shape data. *Methods in Ecology and Evolution* **4**, 393–399 (2013).
- 1077 51.Wickham, H. *Ggplot2: Elegant graphics for data analysis*. (Springer New York, 2009).
1078 at <<http://had.co.nz/ggplot2/book>>
- 1079 52.Wilke, C. O. *cowplot: Streamlined Plot Theme and Plot Annotations for ggplot2*. (2015).
1080 at <<http://cran.r-project.org/web/packages/cowplot/index.html>>

₇₁₅ **Tables**

₇₁₆ **Table 1:** Luciferases used in this study.

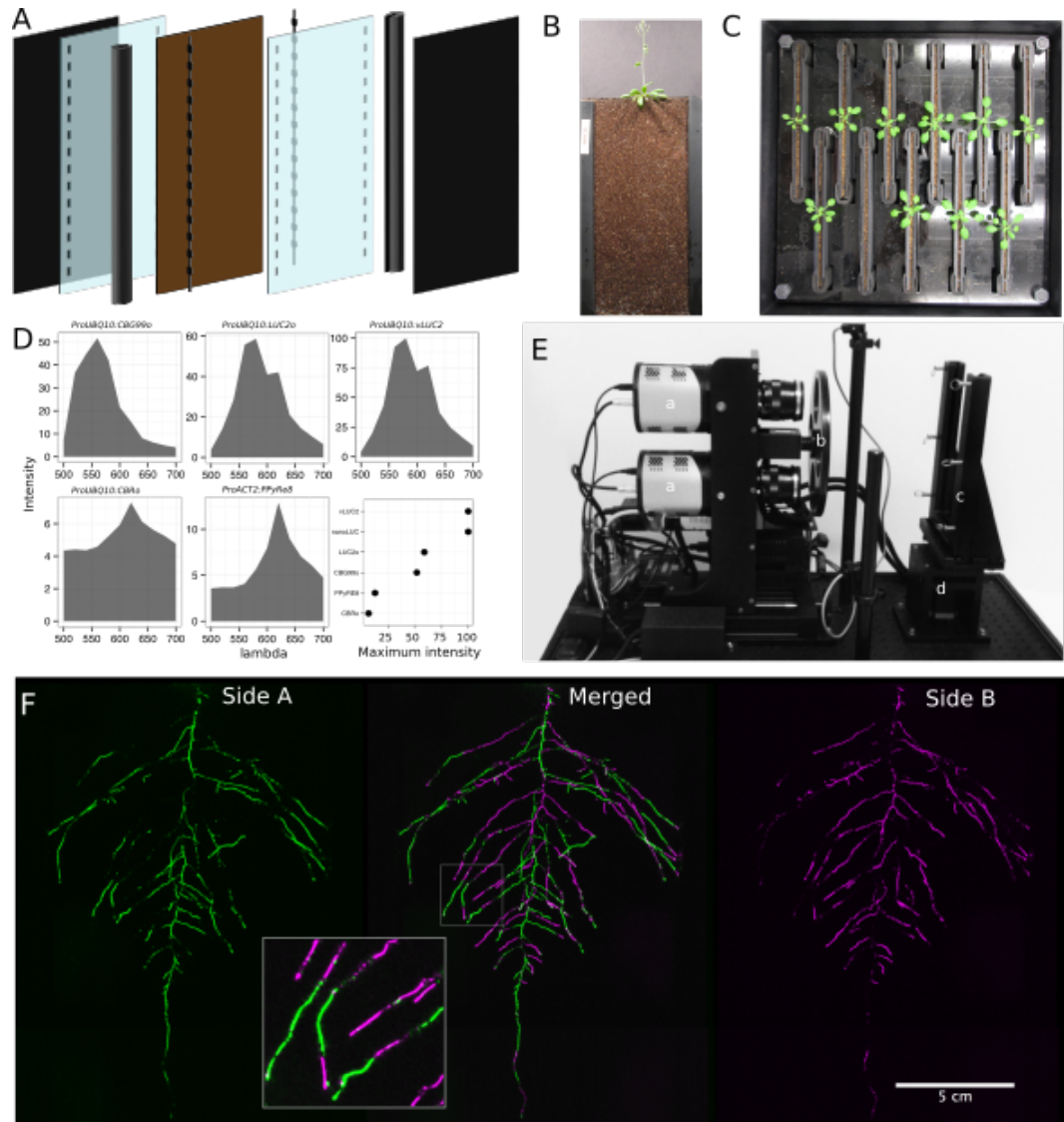
Luciferase	Origin	maximum wavelength	Substrate
Ppy RE8	firefly	618	D-luciferin
CBGRed	click beetle	615	D-luciferin
venus-LUC2	FP + firefly	580	D-luciferin
LUC(+)	firefly	578	D-luciferin
CBG99	click beetle	537	D-luciferin
lux operon	A. fischeri	490	biosynthesis pathway encoded within operon
nanoLUC	Deep sea shrimp	470	furimazine

₇₁₇ **Table 2:** list of root system features extracted using GLO-RIA.

variable	unit
projected area	cm ²
number of visible roots	-
depth	cm
width	cm
convex hull area	cm ²
width	cm
feret	cm
feret angle	°
circularity	-
roundness	-
solidity	-
center of mass	cm
Directionality	°
Euclidean Fourier Descriptors	-

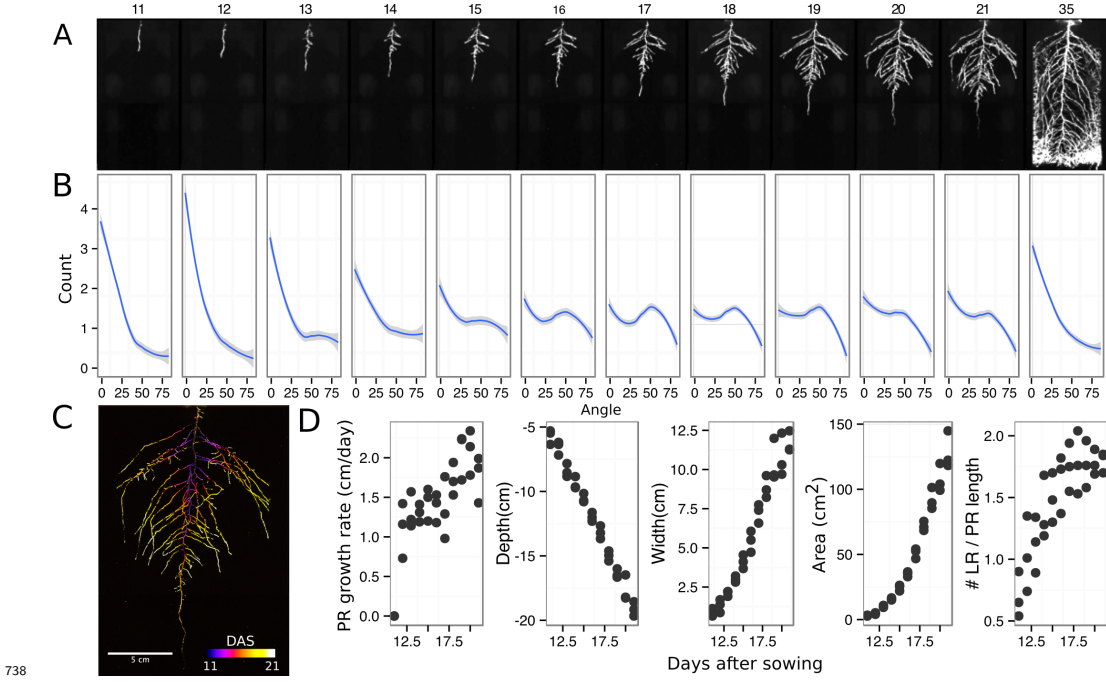
variable	unit
Pseudo landmarks	-

718 **Figures**

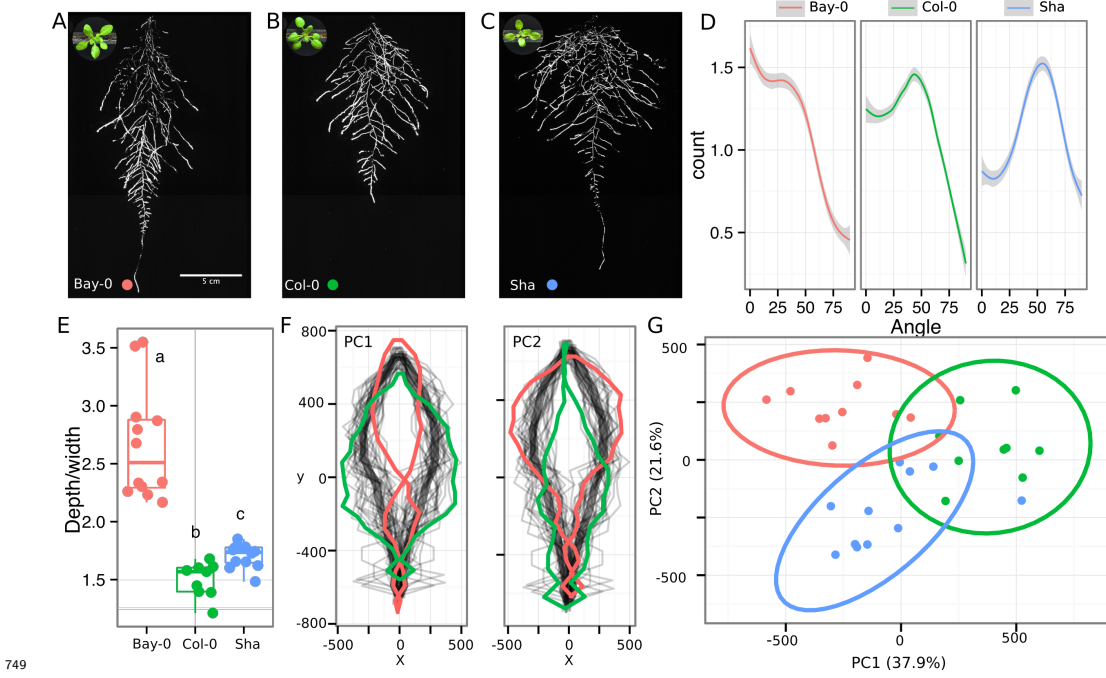


719
 720 **Figure 1. GLO-Roots growth and imaging systems** A) 3D representation of the
 721 different physical components of the rhizotron: plastic covers, polycarbonate sheets,
 722 spacers and rubber U-channels. Blueprints are provided in Supplementary material 1. In brown,
 723 soil layer. B) Thirty five day-old plant in rhizotron with black covers removed. C) Top view
 724 of holding box with eleven rhizotrons. D)In vivo emission spectra of different luciferases
 725 used in this study. Transgenic homozygous lines expressing the indicated transgenes were

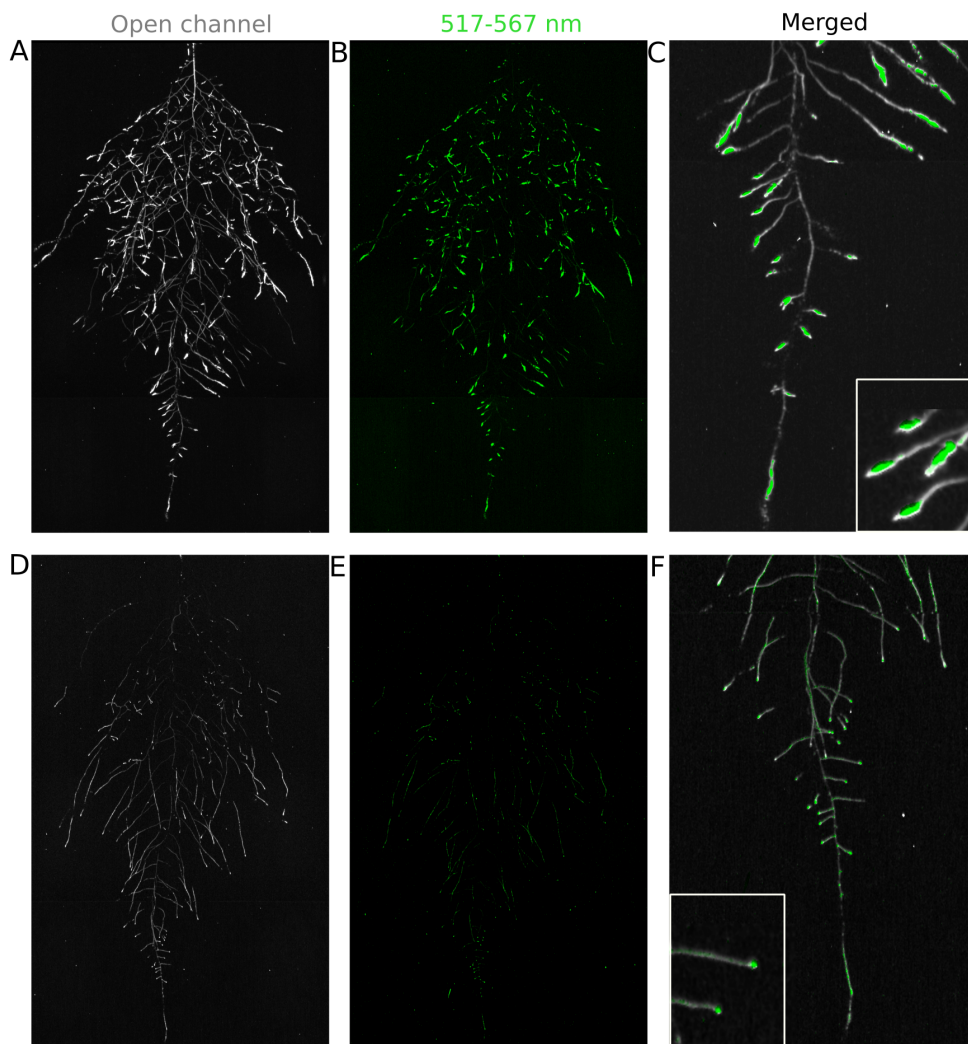
726 grown on agar media for 8 days. Luciferin (300 μ M) was sprayed on the seedlings and
727 plates were kept in the dark and then imaged for 2 s at wavelengths ranging from 500
728 to 700 nm. Five intensity values were taken from different parts of the roots of different
729 seedlings and averaged. Relative maximum intensity values are indicated in the lower right
730 graph. E) GLO 1 imaging system. The system is composed by two back illuminated CCD
731 cameras (a) cooled down to -55 °C. A filter wheel (b) allows for spectral separation of the
732 different luciferases. On the right, a rhizotron holder (c) is used to position the rhizotrons
733 in front of the cameras. A stepper motor (d) rotates the rhizotron 180° to image both
734 sides. F) A 21 DAS plant expressing *ProUBQ10:LUC2o* was imaged on each of two sides
735 of the rhizotron; luminescence signal is colorized in green or magenta to indicate side. In
736 the middle of the panel, a combined image of the two sides is shown. The inset shows a
737 magnified part of the root system. FW: fresh weight, PR: Primary root.



739 **Figure 2. Time-lapse imaging of root systems and quantification using GLO-**
 740 **RIA.** A) Typical daily time-lapse image series from 11 to 35 DAS of a *ProUBQ10:LUC2o*
 741 Col-0 plant. B) Directionality of the root system of plants in panel A calculated using the
 742 directionality plugin implemented in GLO-RIA. C) Color coded projection of root growth
 743 using the images in panel A. D) Primary root growth rate, depth, width, root system area
 744 are automatically calculated from the convex hull, which is semi-automatically determined
 745 with GLO-RIA. Lateral root number and number of lateral roots divided by the primary
 746 root length were quantified manually. A Local Polynomial Regression Fitting with 95%
 747 confidence interval (grey) was used to represent the directionality distribution curve. (0° is
 748 the direction of the gravity vector).



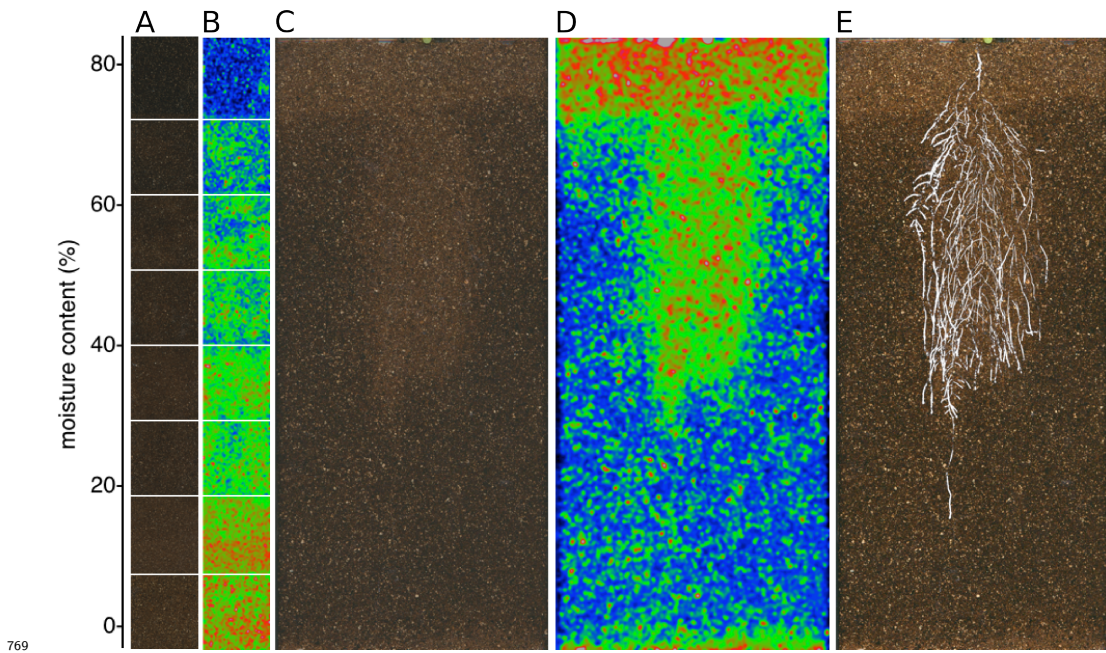
749 **Figure 3. Variation in root architecture between accessions of *Arabidopsis*.** Rep-
 750 resentative root and shoot images of A) Bay-0, B) Col-0 and C) Sha accessions transformed
 751 with *_ProUBQ10:LUC2o_* and imaged after 22 DAS. D) Directionality of the root systems,
 752 E) depth/width ratio, F) Pseudo-landmarks describing shape variation in root system archi-
 753 tecture. Eigenvalues derived from the analysis of 9-12 plants per accession is shown. The
 754 first two Principal Components explaining 38% (PC1) and 22% (PC2) of the shape variation
 755 are plotted. PC1 captures homogeneity of root system width along the vertical axis and
 756 PC2 a combination of depth and width in top parts of the root system. Red and green
 757 lines indicate -3SD and +3SD (Standard Deviations), respectively G) PC separation of the
 758 different ecotypes using the PCs described in (F). A Local Polynomial Regression Fitting
 759 with 95% confidence interval (grey) was used to represent the directionality distribution
 760 curve. 0° is the direction of the gravity vector. Wilcoxon test analysis with $p < 0.01$ was
 761 used to test significant differences between the different accession ($n = 9-12$ plants).

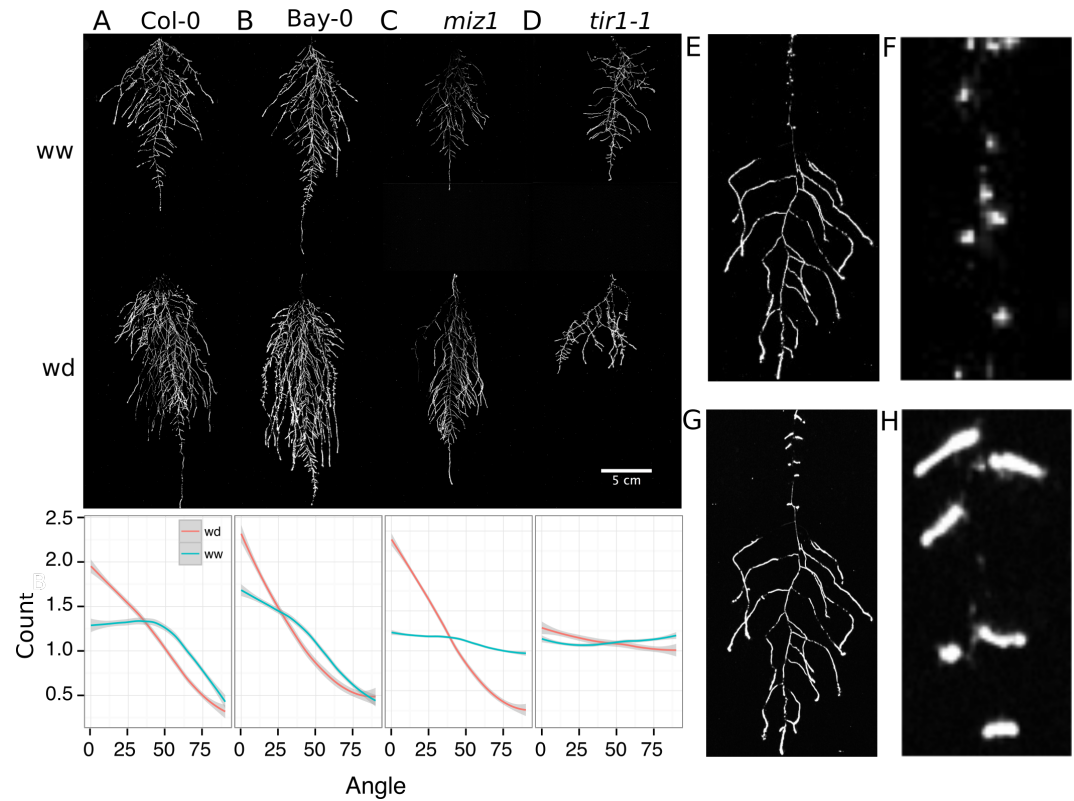


763

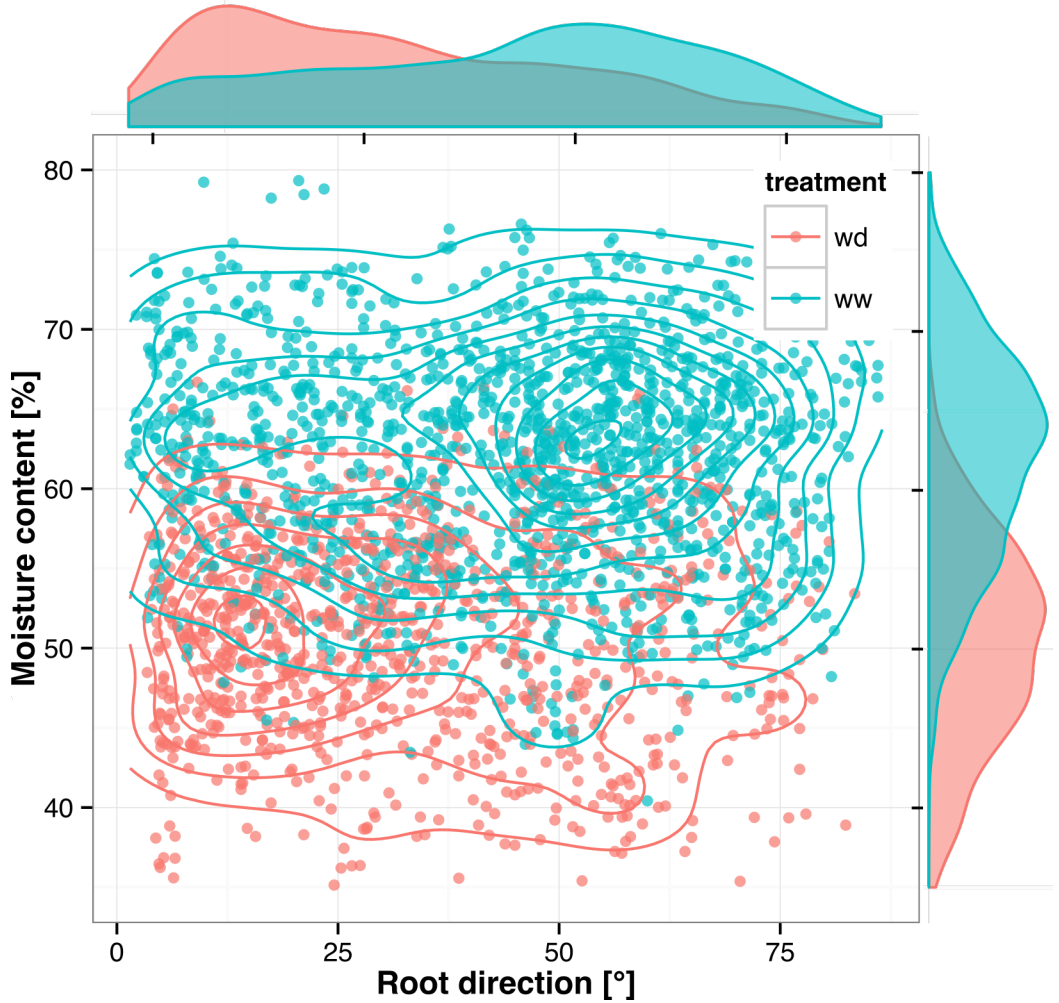
764 **Figure 4. Dual-color reporter visualization of structure and gene expression.**

765 Images of whole root systems (A, D) or magnified portion of roots (C, F) at 22 DAS
 766 expressing *ProDR5rev:LUC+* (green, A, B) or *ProZAT12:LUC* signal (green, D, E) with
 767 skeletonized representation of roots generated using the *ProACT2:PpyRE8o* reporter
 768 expression (in grey).



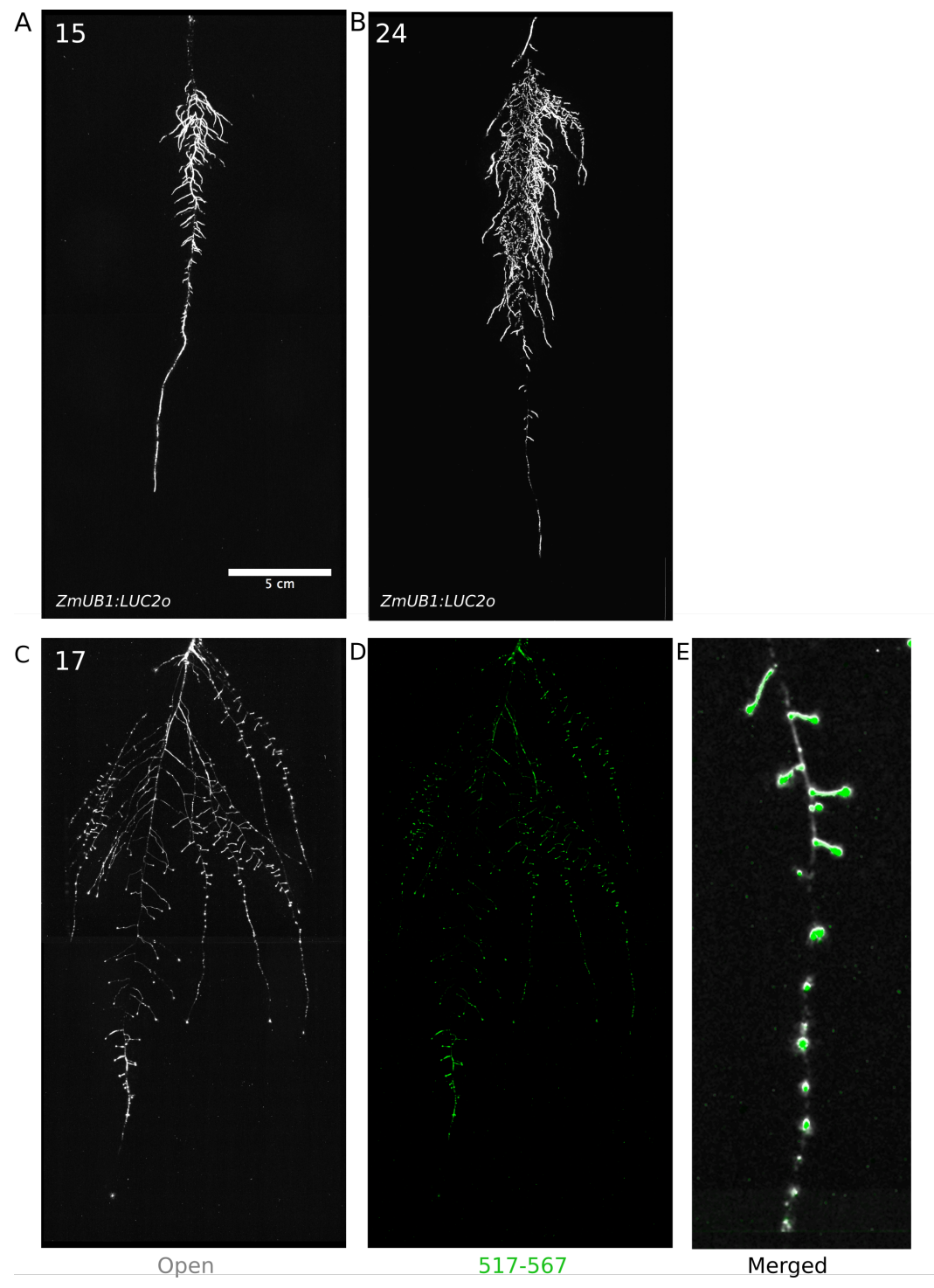


777 **Figure 6. Study of effect of water deficit on root system architecture.** A-D)
 778 Root systems 22 DAS and exposed to water deficit 13 DAS onwards. Sample images of
 779 well watered (left panels) and water deficit (right panels) root systems treated from 13
 780 DAS and directionality (line graphs to left of images) for (A) Col-0 (B) Bay-0 (C) *miz1*
 781 mutant and (D) *tir1-1*. E) Root system of a 22 DAS plant exposed to water deprivation
 782 from 9 DAS onwards with magnified view of lateral root primordia (F). G) The same
 783 root as in (E) 24 hours after rewetting and magnified view of lateral root primordia (H).
 784 Kolmogorov-Smirnov test at $p < 0.001$ was used to compare directionality distributions
 785 between the different treatments and genotypes. A Local Polynomial Regression Fitting
 786 with 95% confidence interval (grey) was used to represent the directionality distribution
 787 curve. 0° is the direction of the gravity vector.
 788



789

790 **Figure 7.** Relationship between local soil moisture content and root growth
 791 direction. Data quantified from the time lapse series shown in [Video 2](#). Density plots
 792 shown at periphery of graph for root direction (x-axis) and soil moisture (y-axis). 0° is
 793 the direction of the gravity vector. Data represents 2535 root tips measured in a series
 794 encompassing 10 time points.



796 **Figure 8:** Roots of *Brachypodium distachyon* transformed with *ProZmUB1:LUC2o* and

797 imaged at 15 (A) and 24 (B) DAS grown in control conditions. C) Open channel of 17
798 DAS tomato plant transformed with *ProeDR5rev:LUC2o* and *Pro35S:PPyRE8o* D) Green
799 channel showing only *ProeDR5rev:LUC2o* E) Amplification of the open and green channel
800 showing increased expression of *ProeDR5rev:LUC2o* reporter in early-stage lateral roots.

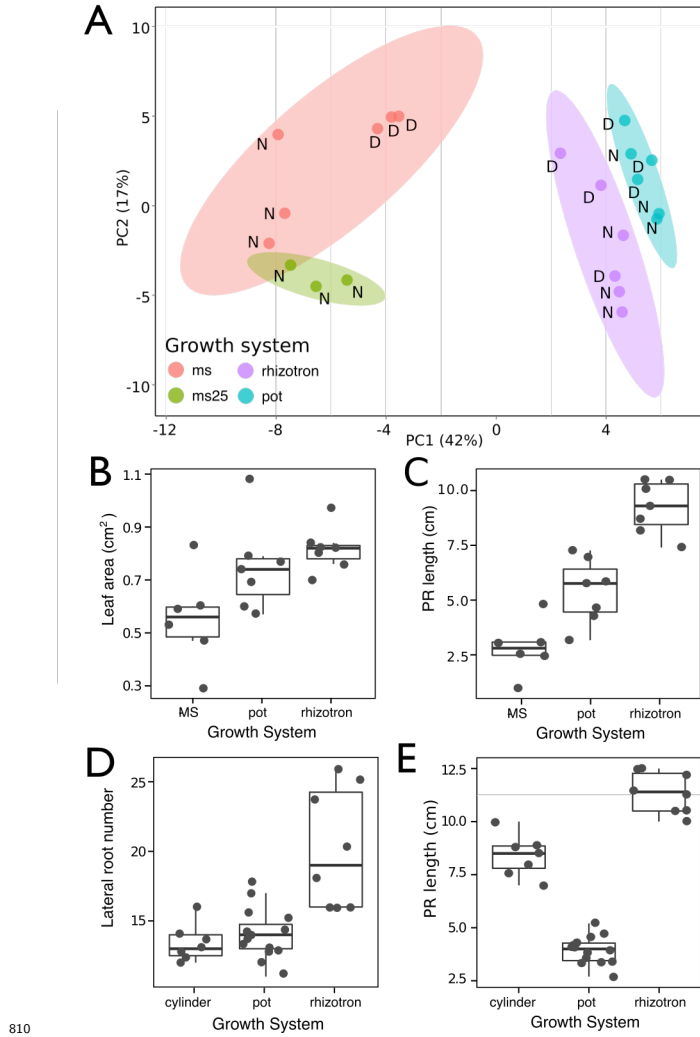
801 **Videos**

802 **Video 1** Time lapse from 11 to 21 DAS of a Col-0 plant expressing ProUBQ10:LUC2o
803 grown in control conditions

804 **Video 2** Time lapse from 16 to 24 DAS of Col-0 plants expressing *ProUBQ10:LUC2o*
805 growing in water deficient (left) and control (right) conditions. Plants were sown under
806 control conditions and water deficit treatment started 11 DAS. Images were taken every
807 day.

808 **Supplementary Material**

809 **Supplementary figures**



810
 811 **Figure 1-figure supplement 1. Effect of different growth systems on plant biol-**
 812 **ogy.** A) Principal Components Analysis (PCA) score plot of a set of 76 genes analyzed by
 813 qPCR from root samples of plants grown in MS plates, pots, and rhizotrons. After 15 DAS
 814 three plants were collected at the end of the day (D) and three were collected at the end of
 815 the night (N). (ms = plant grown in full ms and 1% sucrose, ms25 = plants grown in 25%
 816 of full ms) B) Lateral root number and G) primary root length of 18 DAS plants grown in

⁸¹⁷ 30 cm tall cylinders, pots and rhizotrons, all with a volume of 100 cm³ (n = 6-12 plants).
⁸¹⁸ D) Leaf area and E) primary root length of plants of the same age (15 DAS) as the ones
⁸¹⁹ used for the qPCR experiment (n= 6-7). ANOVA analysis with p < 0.01 was used to test
⁸²⁰ significant differences between the different parameters.

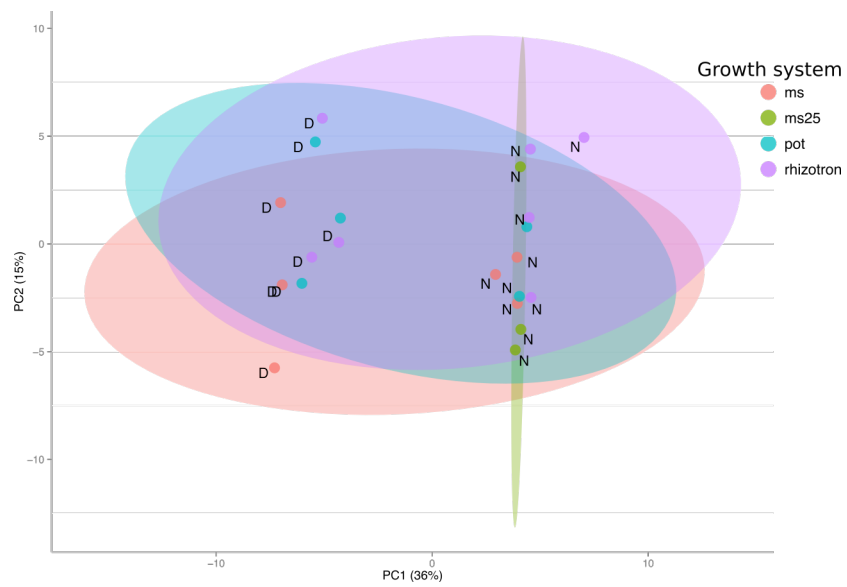
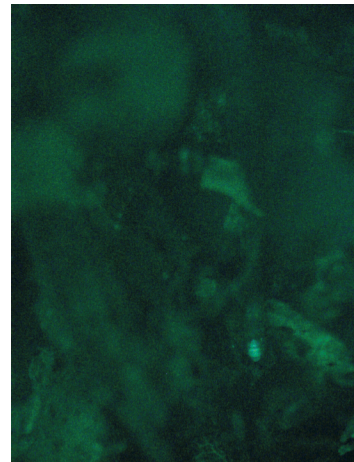


*Figure 1-figure supplement 2. PCA plot of shoots of the same samples analyzed in Figure 1. See Figure 1 for more details regarding experimental conditions used.



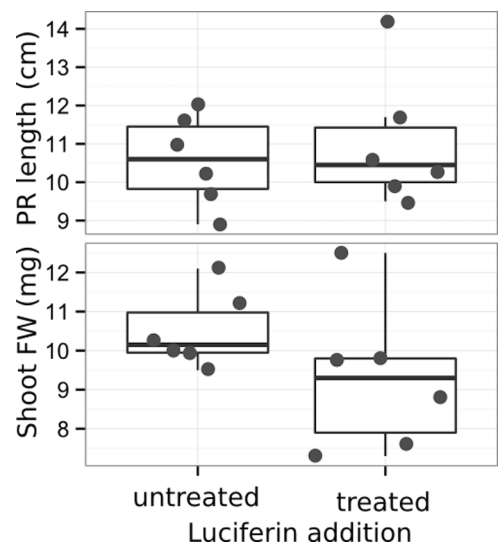
Brightfield

824

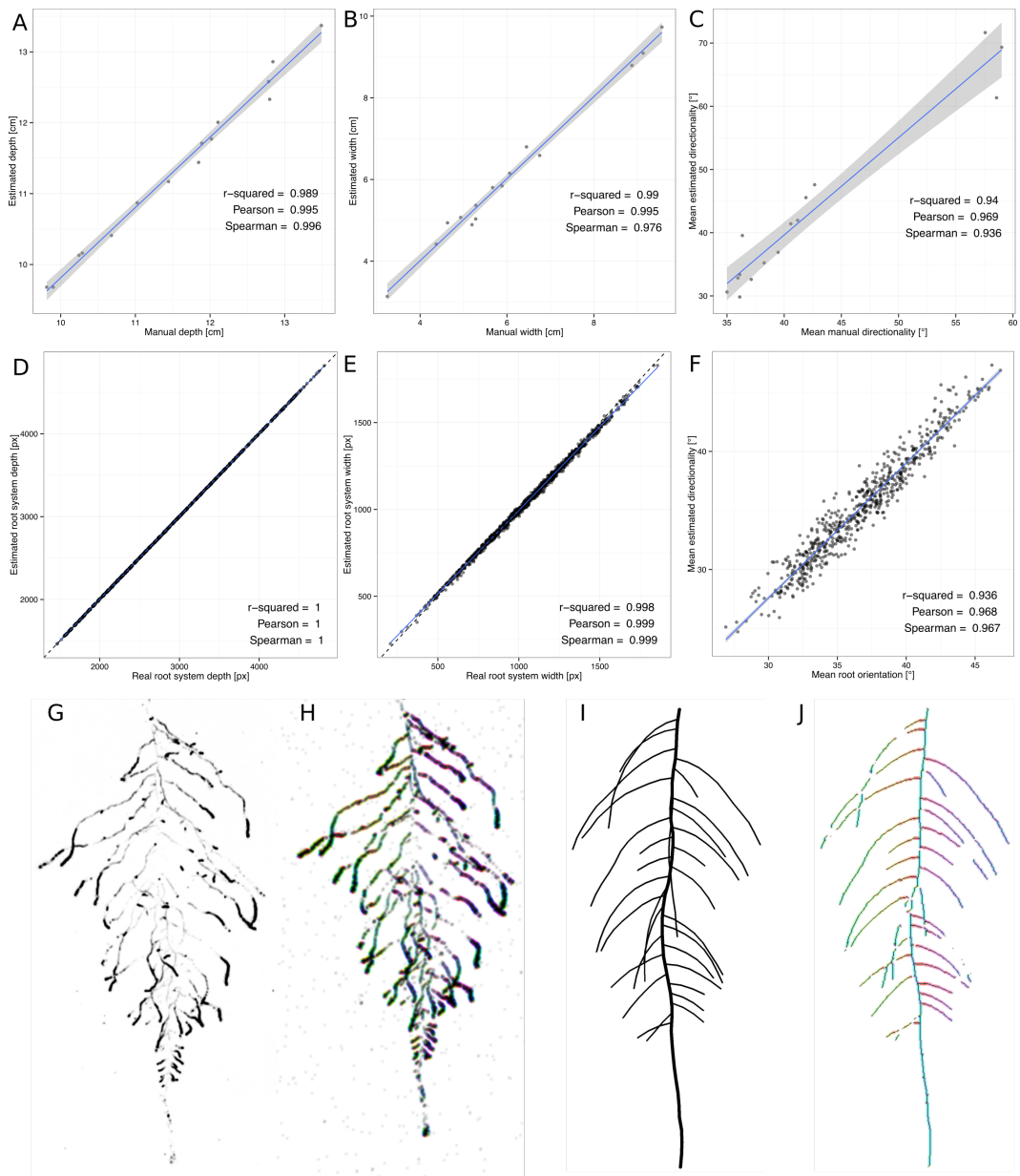


GFP

825 **Figure 1-figure supplement 3** Image of an Arabidopsis root in soil imaged with white
826 light (brightfield) or epifluorescence.



827
828 **Figure 1-figure supplement 4** Effect of luciferin addition on primary root length and
829 shoot size of 14 DAS seedlings that were either continuously exposed to 300 μ M luciferin
830 from 9 DAS after sowing or not.



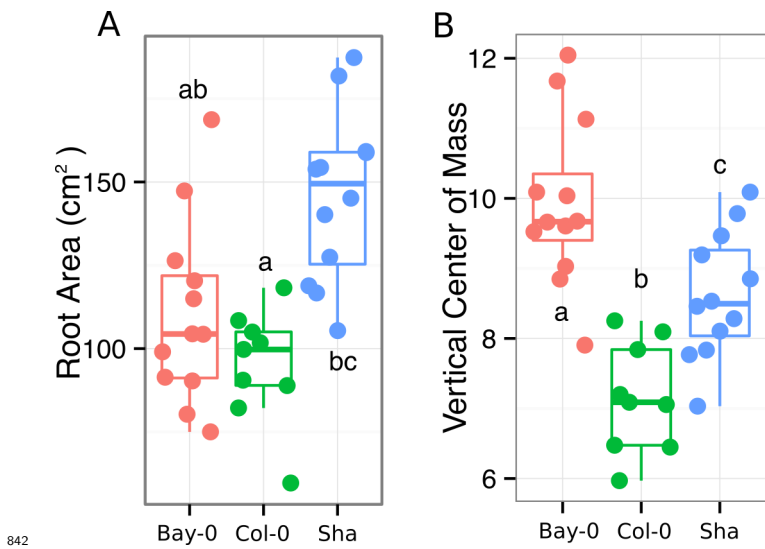
831

832 **Figure 1-figure supplement 5 GLO-RIA validation.** Validation was carried out using
 833 two approaches. We first used manually quantified root system depth (A) width (B)
 834 and average lateral root angles (C) in a set of 15 root systems corresponding to different
 835 *Arabidopsis* accessions. We then generated 1240 contrasting root systems using ArchiSimple
 836 as a ground truth to validate root system depth (D) width (E) and directionality (F).

837 Example of a real (G) and ArchiSimple generated (H) root systems and corresponding

838 GLO-RIA color-coded directionality (I, J).

⁸³⁹ **Figure 1-figure supplement data 1:** Two way ANOVA P-values comparing plants grown
⁸⁴⁰ in MS media vs. plants grown in soil (pots or rhizotrons) and plants collected at day or night.
⁸⁴¹ We used p-value < 0.00065 threshold based on Bonferoni adjustment for multiple testing.



843 **Figure 3-figure supplement 1** A) root area, B) vertical center of mass of Bay-0, Col-0
 844 and Sha accessions.

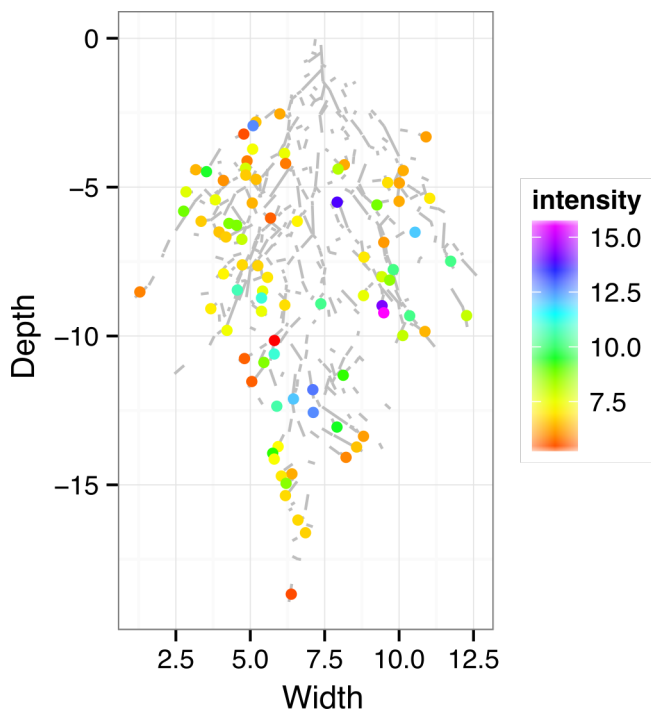
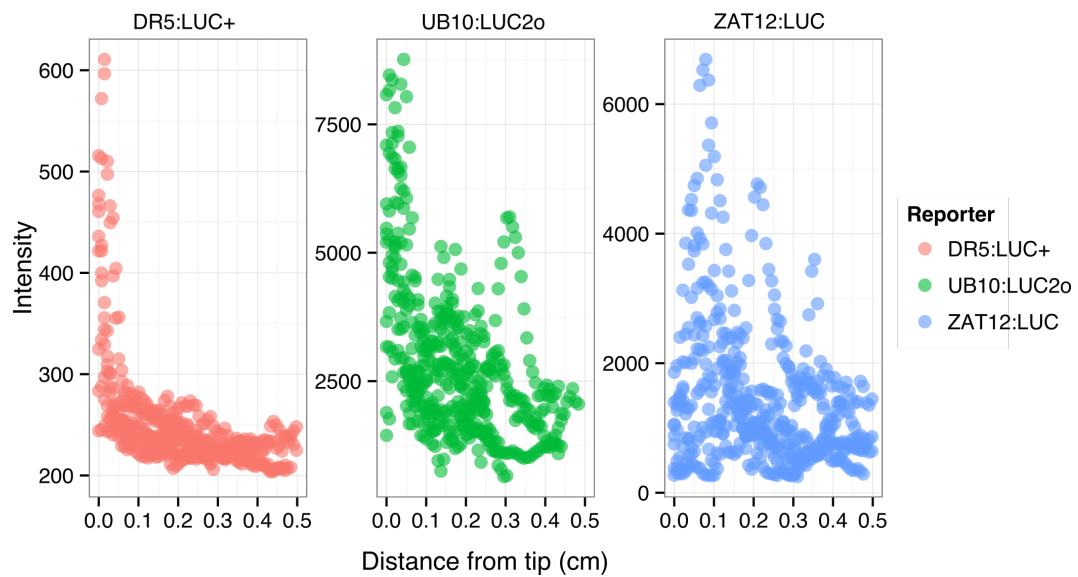


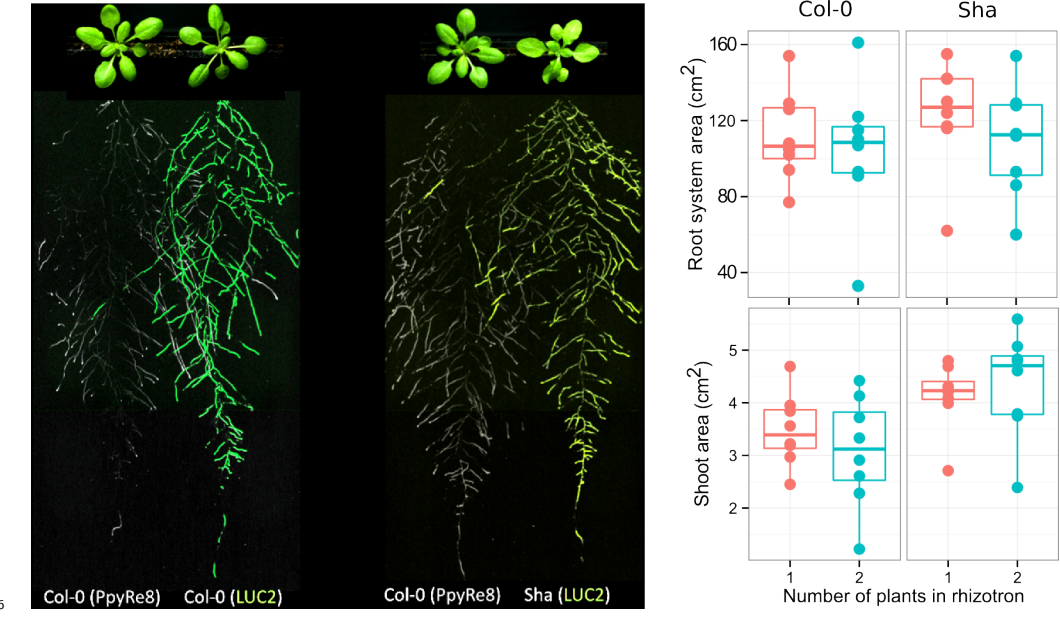
Figure 4-figure supplement 1:

845 ZAT12:LUC intensity and root segments automatically identified values along the root tip.
 846
 847 Data was manually obtained by obtaining the intensity profile of the first 0.5 cm from the
 848 root tip of individual lateral roots. Ten lateral roots for each reporter were measured.
 849



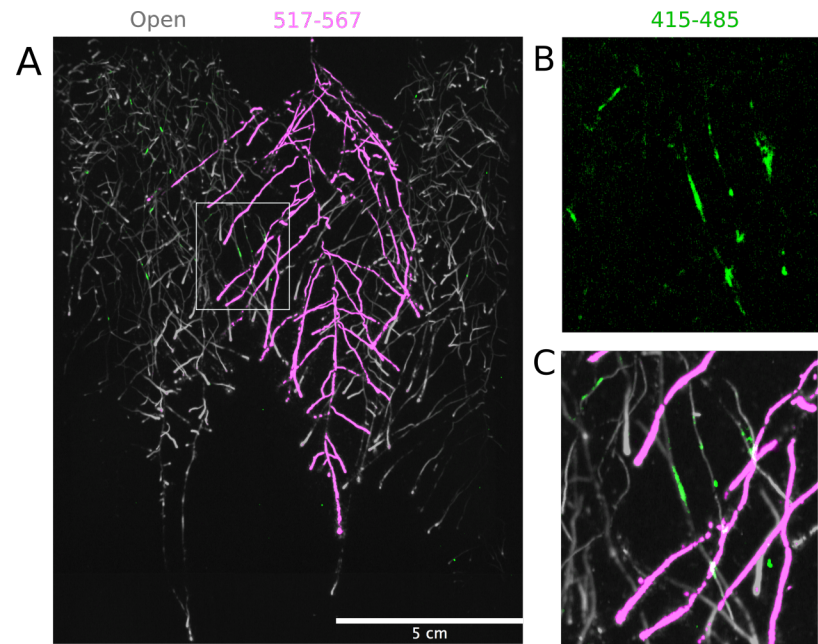
850
851 **Figure 4-figure supplement 2:** DR5:LUC+, UBQ10:LUC2o and ZAT12:LUC intensity
852 values along the root tip. Data was manually obtained by obtaining the intensity profile
853 of the first 0.5 cm from the root tip of individual lateral roots. Ten lateral roots for each
854 reporter were measured.

855



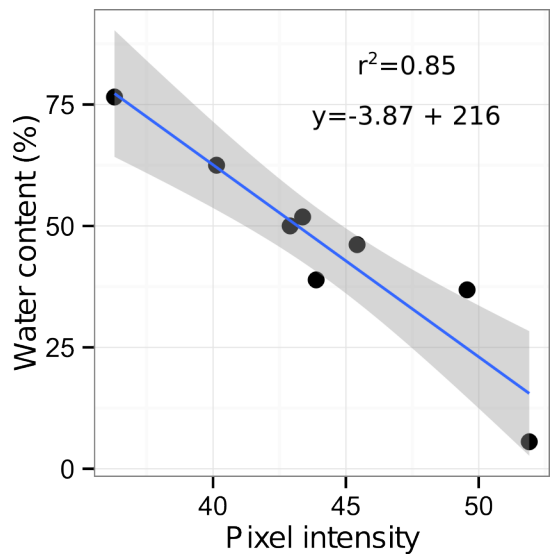
856
857 **Figure 4-figure supplement 3.** Images of plants at 22 DAS growing in the
858 same rhizotron and expressing different luciferases. A) Two Col-0 plants expressing
859 *ProUBQ10:LUC2o* and *ProACT2:PPyRE8o* B) Col-0 plant expressing *ProACT2:PPyRE8o*
860 and Sha plant expressing *ProUBQ10:LUC2o*.

861



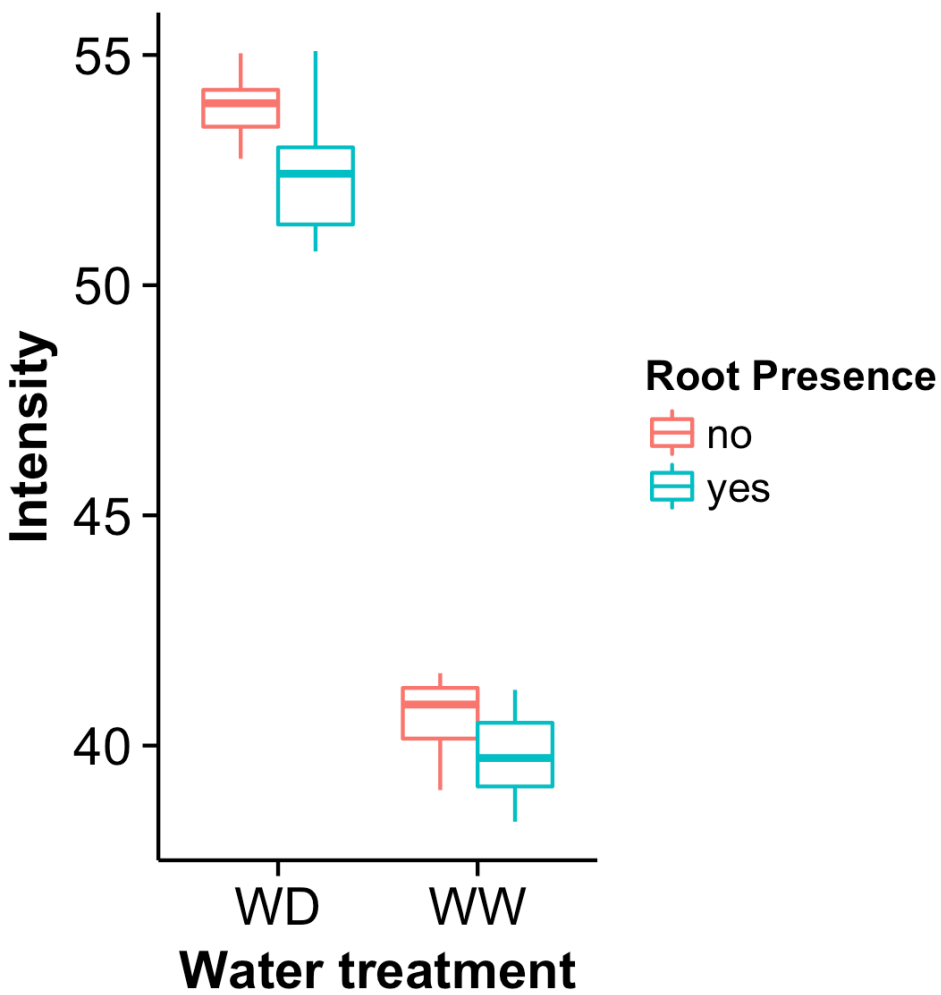
863 **Figure 4-figure supplement 4. Three-reporter-based analysis of root-root-**
 864 **microbe interactions.** A) Image showing a 22 DAS *ProUBQ10:LUC2o* plant (magenta)
 865 grown in the same rhizotron with *ProACT2:PpyRE8o* plants (grey). Plants were inoculated
 866 with *Pseudomonas fluorescens* CH267 (green). Magnified portion of root systems colonized
 867 by *Pseudomonas fluorescens* showing *P. fluorescences* (B) only or all three reporters
 868 together (C).

869

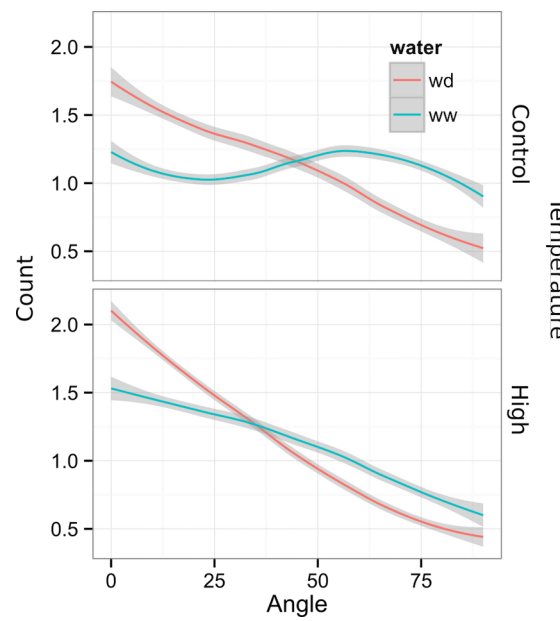


870 **Figure 5-figure supplement 1:** Moisture calibration curve. Rhizotrons with different
871 levels of moisture were prepared and scanned to obtain readings of pixel intensity. Soil from
872 rhizotrons was then weighed, dried down in an oven at 70 °C for 48 hours and percent water
873 content quantified.
874

875

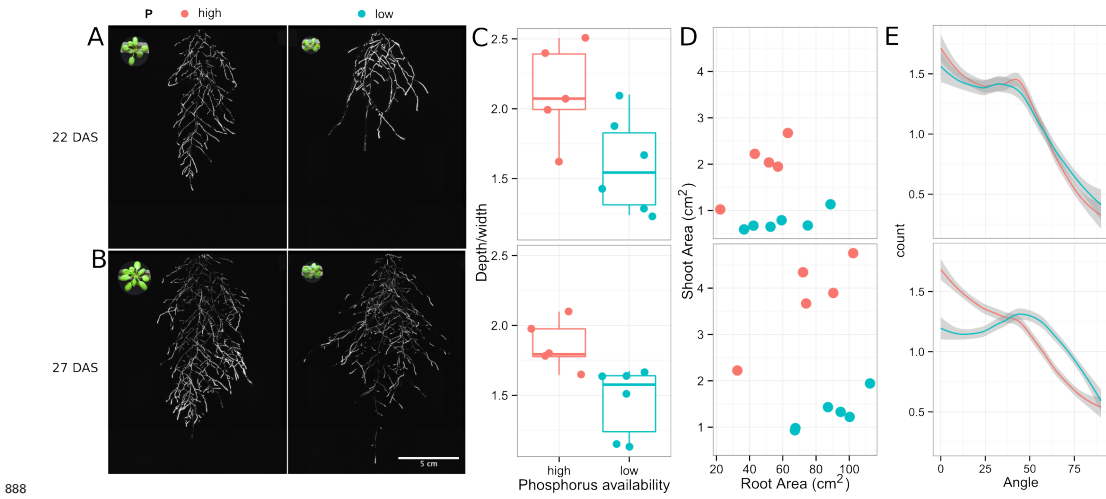


876
877 **Figure 5-figure supplement 2.** Comparison of soil intensity values between
878 **areas of the rhizotron with or without the presence of roots, determined based**
879 **on luminescence data.** Mean intensity values from 100 x 100 pixel squares samples of
880 both areas were obtained from 10 different rhizotrons. Wilcoxon test analysis with $p < 0.01$
881 was used to test significant differences between areas with our without root presence.
882



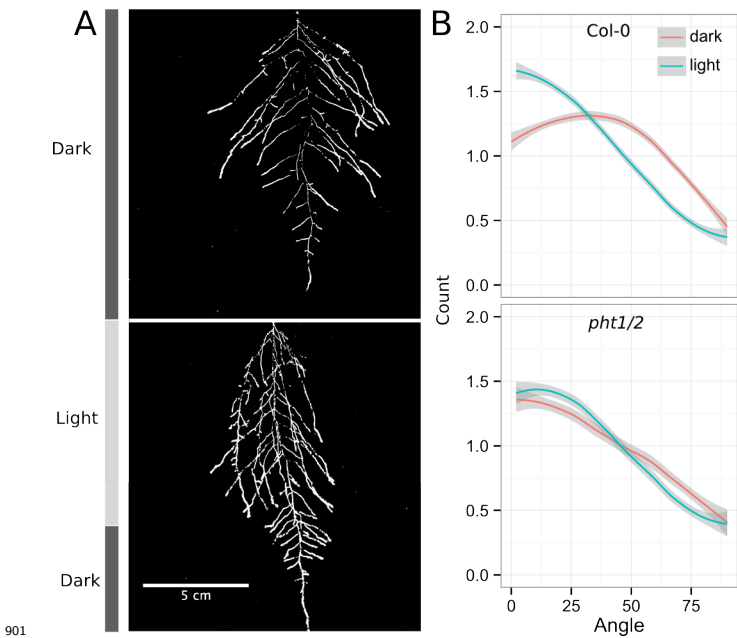
883
884 **Figure 6-figure supplement 1** Directionality analysis of roots of plants transferred to
885 water deprivation conditions after 9 DAS and kept 22 °C (control temperature) and 29 °C
886 (high temperature) until 22 DAS. (0° is the direction of the gravity vector).

887

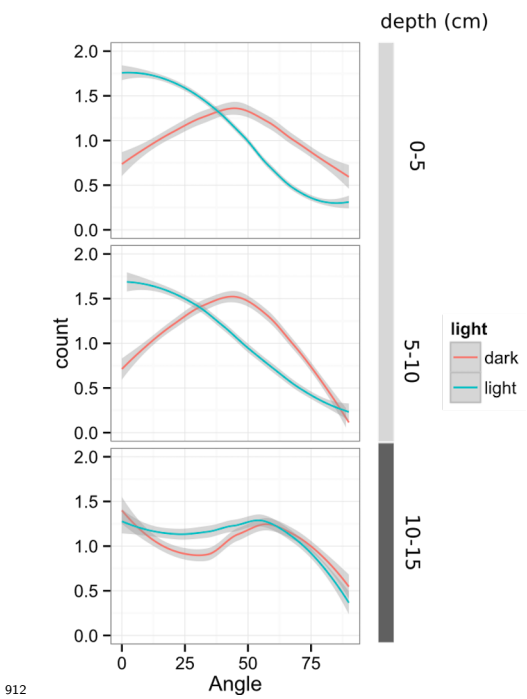


889 **Figure 6-figure supplement 2. Phosphorus deficiency response of root systems**
890 Shoot and root systems of *ProUBQ10:LUC2o* Col-0 plants growing in soil supplemented
891 with 1ml of 100 μM P-Alumina (left) and 0-P-Alumina (right) 22 (A) or 27 (B) DAS. C)
892 Root depth/width ratio of 22 (top) and 27 (bottom) DAS plants. D) Scatter-plot showing
893 relationship between root and shoot system area at 22 (top) and 27 (bottom) DAS. E)
894 Root directionality distribution in plants 22 (top) and 27 (bottom) DAS. Anova analysis at
895 $p < 0.01$ was used to compare depth/width ratios in P treatments. Kolmogorov-Smirnov
896 test at $p < 0.001$ was used to compare directionality distributions between the different
897 treatments. A Local Polynomial Regression Fitting with 95% confidence interval (grey)
898 was used to represent the directionality distribution curve.(0° is the direction of the gravity
899 vector).

900

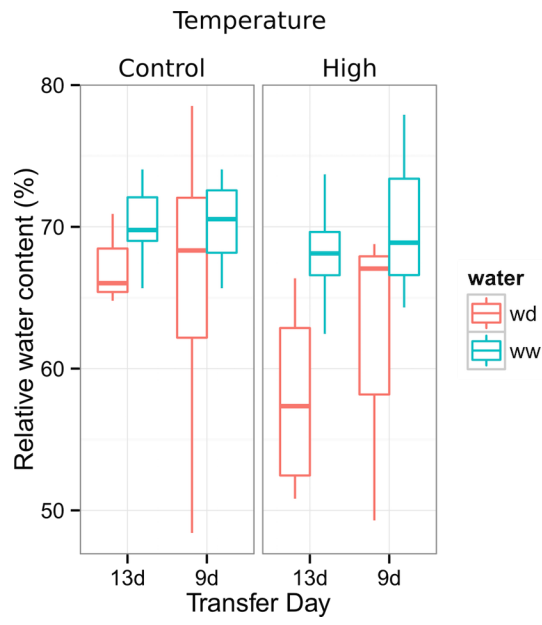


902 **Figure 6-figure supplement 3. Effect of light on root directionality.** A) Col-0
903 root systems shielded (top) or light exposed (bottom). After 9 DAS the top third of the
904 rhizotron was exposed to light (indicated on the side with a light grey bar) and plants were
905 imaged at 20 DAS. B) Directionality analysis of root systems shielded (red) or exposed
906 (green) to light for Col-0 (top panel) or *pht1/2* double mutant (bottom panel). Between
907 4 and 6 plants were analyzed per treatment. ANOVA analysis at $p < 0.01$ was used to
908 compare depth/width ratios in P treatments. Kolmogorov-Smirnov test at $p < 0.001$ was
909 used to compare directionality distributions between the different treatments. A Local
910 Polynomial Regression Fitting with 95% confidence interval (grey) was used to represent
911 the directionality distribution curve. (0° is the direction of the gravity vector).

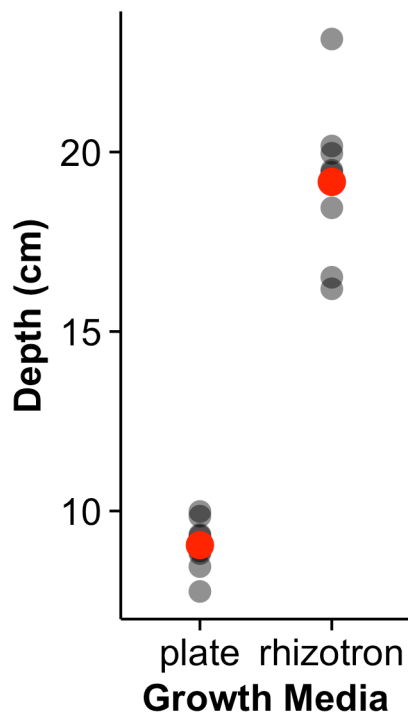


912 **Figure 6-figure supplement 4** Plots showing output of directionality analysis performed
 913 at different depths (0-5, 5-10, 10-15 cm) in rhizotrons exposed to light or kept in the dark.
 914 (0° is the direction of the gravity vector).
 915

916



917 **Figure 6-figure supplement 5.** Leaf relative water content of 23 DAS plants that
 918 were subjected to water deprivation (WD) after 9 or 13 DAS or kept under
 919 well watered (WD) conditions. At 9 DAS half of the plants were kept under control
 920 temperature conditions (22 °C) and the other half transferred to a 29 °C (high) chamber. n
 921 = 6-8 plants.
 922
 923



924

925 **Figure 8-figure supplement 1** Depth of the primary root of *Brachypodium* plants grown

926 in rhizotrons or on gel-based media (n=8-11).

927

928 **Supplementary material**

929 **Supplemental Material 1**

930 Blueprints of the holders, clear sheets and spacers needed to built the rhizotrons. Additional
931 details are provided in the materials and methods. Files are provided in Adobe Illustrator
932 .ai and Autocad .dxf formats.

933 **Supplemental Material 2**

934 Primers used in the qPCR experiment.

935 **Supplemental Material 3**

936 Vector maps of all the constructs used in this work.

937 **Source data files**

938 Source data files used for building the following figures are provided: figure_1D.csv
939 figure_1_figure_supplement_1A-B.csv
940 figure_1_figure_supplement_1C_D.csv
941 figure_1_figure_supplement_1E-F.csv
942 figure_1_figure_supplement_2.csv
943 figure_1_figure_supplement_3.csv
944 figure_2C.csv
945 figure_2D.csv
946 figure_3D.csv
947 figure_3E.csv
948 figure_3F-G_1.csv
949 figure_3F-G_2.tps
950 figure_3_figure_supplement_1A-B.csv
951 figure_4G_reporter.csv
952 figure_4G_root_segment.csv
953 figure_4_figure_supplement_1.csv

```
954 figure_4_figure_supplement_2.csv  
955 figure_5_figure_supplement_1.csv  
956 figure_6_A-D.csv  
957 figure_6_figure_supplement_2-C-D.csv  
958 figure_6_figure_supplement_2-E.csv  
959 figure_6_figure_supplement_3.csv  
960 figure_6_figure_supplement_4.csv  
961 figure_6_figure_supplement_5.csv  
962 figure_7.csv  
963 figure_8_figure_supplement_1.csv
```